Journal Pre-proofs

Route-aware detection of ship collision avoidance manoeuvres via change point analysis with intention inference

Boyuan Zhang, Hao Rong, Huanhuan Li, Zaili Yang

PII: S1366-5545(26)00599-5
DOI: https://doi.org/10.1016/j.tre.2026.105261
Reference: TRE 105261

To appear in: *Transportation Research Part E*

Received Date: 21 March 2026
Revised Date: 25 July 2026
Accepted Date: 13 September 2026

Please cite this article as: Zhang, B., Rong, H., Li, H., Yang, Z., Route-aware detection of ship collision avoidance manoeuvres via change point analysis with intention inference, *Transportation Research Part E* (2026), doi: https://doi.org/10.1016/j.tre.2026.105261

Route-Aware Detection of Ship Collision Avoidance Manoeuvres via Change Point Analysis with Intention Inference

Boyuan Zhang [a], Hao Rong [a,*], Huanhuan Li [b], Zaili Yang [a,*]

[a] Liverpool Logistics, Offshore and Marine Research Institute, Liverpool John Moores University, Liverpool, UK

[b] School of Engineering, University of Southampton, Southampton, UK

* Corresponding authors: h.rong@ljmu.ac.uk (Hao Rong), z.yang@ljmu.ac.uk (Zaili Yang)

Acknowledgement

This project has received funding from the European Research Council (ERC) under the European Union's Horizon 2020 research and innovation programme (Grant Agreement No. 864724).

Route-Aware Detection of Ship Collision Avoidance Manoeuvres via Change Point Analysis with Intention Inference

Abstract: Reliable and human-consistent collision avoidance is essential for Maritime Autonomous Surface Ships (MASS) operating in mixed traffic environments. A key challenge is the extraction of representative critical encounter scenarios from real-world data without relying on predefined risk thresholds or expert-driven rules. This study proposes a data-driven, route-aware framework for detecting ship collision avoidance behaviours and extracting the critical encounter scenarios in which such behaviours occur. The framework comprises three components. First, ship motion patterns are analysed to characterise normal route-following behaviour, enabling collision avoidance behaviour to be distinguished from routine navigation. Second, a unified cost function is formulated to jointly evaluate multiple kinematic features while explicitly incorporating planned route information, enabling separation of route-following course changes from potential avoidance actions. Change Point Detection (CPD) method is then applied to identify behavioural transitions and segment ship trajectories into candidate collision avoidance manoeuvres. Third, an intention-informed encounter identification approach is introduced, where avoidance intent is inferred by comparing observed trajectories with virtual route-following trajectories. This enables confirmation of true collision avoidance behaviour and extraction of the associated critical encounter scenarios. The proposed method is validated using Automatic Identification System (AIS) data from the high-traffic Øresund region, including the Helsingør-Helsingborg ferry corridor. Results on a labelled dataset show strong performance, achieving an F1-score of 0.8203 and 0.7443 in behaviour identification and encounter extraction, respectively. The findings demonstrate that the framework can robustly identify avoidance manoeuvres and capture critical encounters. Moreover, the proposed behaviour identification method is further applied in various navigational environments to verify its generalisation. The proposed critical encounter extraction framework provides empirically grounded insights into MASS development and testing, maritime situational awareness enhancement, and traffic management.

Keywords: Collision Avoidance Behaviour, Critical Encounter, AIS data mining, Maritime Autonomous Surface Ships, Change Point Detection.

1. Introduction

The rapid development of smart shipping and Maritime Autonomous Surface Ships (MASS) is driving maritime transportation towards increasingly intelligent and autonomous navigation systems (Li and Yang, 2023; Wang et al., 2024b). However, safe navigation in dense traffic environments remains a critical challenge, as ship collisions can lead to severe human casualties, economic losses, and environmental damage (Feng and Yang, 2026; Guedes Soares and Teixeira, 2001; Yip, 2008). In the foreseeable future, conventional and autonomous ships are expected to coexist in mixed traffic environments. In such environments, autonomous systems need to anticipate and respond to human manoeuvres in a manner consistent with the navigators' intent and practice (Negenborn et al., 2023). Therefore, extracting real-world collision avoidance behaviour from ship trajectories can provide empirical evidence of human navigational interaction behaviour and latent traffic conflict, supporting both MASS development and proactive maritime traffic safety management.

The Automatic Identification System (AIS) data provides large-scale records of ship kinematics and voyage information, including ship dimensions, position, speed, and course, which enables trajectory-based analysis of real-world navigation (Yang et al., 2019). Building on AIS data, a growing body of research has extracted high-level navigational knowledge to support maritime traffic analysis and management, including ship trajectory prediction (Gong et al., 2025; Li et al., 2023; Rong et al., 2019), traffic flow prediction (Chen et al., 2026; Liang et al., 2022; Yuan et al., 2025), traffic pattern extraction (Li et al., 2022; Rong et al., 2022a; Xiao et al., 2019), and abnormal behaviour detection (Liang et al., 2024; Qi et al., 2025; Rong et al., 2024). These studies have provided important support for maritime situational awareness, traffic organisation, and safety monitoring. However, many of them primarily characterise general ship movement patterns or deviations from normal navigation, while the interaction process through which ships resolve potential conflicts remains less explicitly represented. Collision avoidance behaviour differs from general motion patterns because it is triggered by ship-to-ship interactions and reflects how a ship deviates from routine navigation, responds to surrounding ships, and recovers after the conflict has been resolved. Therefore, extracting collision avoidance behaviour from ship trajectories requires not only detecting manoeuvring changes, but also linking these changes to the corresponding ship-to-ship interaction.

In maritime traffic systems, many potentially dangerous ship interactions do not develop into accidents because they are resolved by timely collision avoidance manoeuvres. These successfully resolved conflicts are usually hidden in historical ship trajectories, but they contain important information about where traffic conflicts occur, how ships respond, and which interaction patterns repeatedly challenge navigational safety (Rong et al., 2022a; Xin et al., 2023). Therefore, this study focuses on critical encounter scenarios, defined as ship encounters in which at least one ship conducts an observable collision avoidance manoeuvre during the approaching phase. Existing methods usually identify critical encounters using collision risk indicators (Zhang et al., 2021). Although these methods are useful for detecting potentially risky ship pairs, they do not always verify whether an observed manoeuvre is actually related to collision avoidance, nor do they sufficiently distinguish avoidance-induced manoeuvres from route-following course alterations in structured waterways. As a result, it remains challenging to precisely extract collision avoidance behaviours from ship trajectories and construct behaviourally meaningful critical encounter scenarios for MASS testing, waterway risk analysis, and proactive traffic management.

To address these limitations, this paper proposes a route-aware and intention-informed framework for extracting collision avoidance behaviour and the associated critical encounter scenarios from ship trajectories. The novelty of this study does not lie in the general analysis of ship collision avoidance behaviour, but in the precise extraction of such behaviour from ship trajectories where avoidance manoeuvres are sparse, interaction-driven, and often mixed with route-following movements. The main contributions are threefold:

(1) A behaviour-grounded framework is proposed for extracting critical encounter scenarios from ship trajectories. Rather than identifying critical encounters only through geometric proximity, collision risk indicators, or predefined thresholds, the proposed framework first extracts observable collision avoidance behaviour from ship trajectories and then constructs the associated critical encounter scenarios. This allows the extracted scenarios to preserve empirical ship-to-ship interaction information and provides behaviour-based evidence of latent traffic conflicts.

(2) A route-aware method is developed for the precise extraction of collision avoidance behaviour. The method identifies the complete manoeuvring process of collision avoidance behaviour from ship trajectories, including deviation, recovery, and stabilisation. By incorporating planned-route information as a behavioural baseline, the method distinguishes potential avoidance manoeuvres from routine route-following course alterations, improving the reliability of collision avoidance behaviour extraction in structured waterways.

(3) An intention-informed encounter extraction method is introduced to associate detected avoidance behaviour with target ships. The method links observed manoeuvring behaviour to the surrounding ships being avoided, so that the extracted critical encounters are not only risky in a geometric sense, but are also associated with inferred avoidance intention. This supports the construction of behaviourally meaningful critical encounter scenarios for MASS testing, waterway risk analysis, and proactive maritime traffic management.

The remainder of this paper is organised as follows. Section 2 reviews the existing literature on ship collision avoidance behaviour analysis and critical encounter scenario extraction, and identifies the main research gaps addressed in this study. Section 3 presents the proposed methodology, including the collision avoidance behaviour detection framework, the Change Point Detection (CPD) process, and the intent-based critical scenario extraction method. In Section 4, the experimental settings and the main results of behaviour detection and scenario extraction, and characterisation of the behaviour revealed by the extracted scenarios are reported. Section 5 discusses the implications of the findings and the limitations of the proposed framework. Finally, Section 6 summarises the main conclusions of the study and outlines directions for future research.

2. Literature review

This section reviews the literature from two closely related perspectives. The first perspective concerns ship trajectory analysis for maritime traffic knowledge extraction, which focuses on identifying regular navigation patterns and traffic dynamics from ship trajectories. These studies provide important knowledge about routine ship movements and route-following behaviour, forming the basis for distinguishing normal navigation from interaction-induced manoeuvres. The second perspective concerns critical encounter extraction, which focuses on identifying safety-critical ship-to-ship interactions and collision avoidance behaviours. This stream of research is directly related to the construction of behaviourally meaningful encounter scenarios and the interpretation of how ships respond to potential conflict.

2.1. Ship motion pattern analysis

Ship trajectories provide an important data source for extracting high-level maritime traffic knowledge about routine ship movements, supporting applications such as trajectory prediction and route planning. Merchant ships usually navigate along relatively stable routes shaped by navigational safety, transport efficiency, and operational economy (Yan et al., 2020). These regular routes form the basic structure of maritime traffic and have been widely studied through ship trajectory analysis. Machine learning methods are commonly used to extract ship movement patterns from historical trajectories. For example, Rong et al. (2022a) applied Ordering Points To Identify the Clustering Structure (OPTICS) clustering, Gaussian process, and graph theory methods to extract ship movement patterns and support maritime traffic prediction. Zhang et al. (2021) incorporated both static voyage features and dynamic navigation features, using K-means to cluster trajectories according to origin-destination pairs and voyage length, followed by Density-Based Spatial Clustering of Applications with Noise (DBSCAN) to distinguish trajectories with different movement characteristics. Overall, existing studies show that similarity measurement, feature extraction, and clustering methods can effectively reveal regular route structure and route-following behaviour from historical ship trajectories.

Existing route and traffic pattern extraction studies have used the extracted route information in different maritime applications. For ship route planning, Li and Yang (2023) incorporated AIS data-based machine learning into unsupervised route planning for MASS. Historical AIS trajectories of manned ships were used to extract ship motion patterns, which were then transformed into route planning references through trajectory similarity measurement and clustering. Based on the extracted patterns, representative routes were generated for different ship types, including cargo ships, tankers, and container ships. For abnormal behaviour detection, Rong et al. (2024) proposed a framework for detecting and classifying ship abnormal behaviours using AIS data. Historical trajectories were first used to extract traffic motion patterns and construct route-based normalcy models. Ship abnormal behaviour was then detected by identifying deviations from these normal route-based motion patterns, and abnormal behaviour types were further classified using extracted motion features and a Random Forest classifier. For ship trajectory prediction, Li et al. (2024b) developed a Deep Bi-Directional Information-Empowered (DBDIE) model that integrates the Bi-directional Long Short-Term Memory (Bi-LSTM), the Bi-directional Gated Recurrent Unit (Bi-GRU), and an attention mechanism to predict ship trajectories from historical AIS data. These studies show that route information has been widely used to describe dominant navigation patterns and support data-driven maritime transportation analysis. However, maritime traffic systems are not only characterised by routine route-following movements, but also by ship-to-ship interactions through which potential conflicts are resolved. Existing trajectory-based studies mainly focus on extracting regular routes, modelling normal traffic patterns, supporting route planning, or predicting future ship movements. Relatively limited attention has been paid to how route information can be used to interpret interaction-driven manoeuvring behaviour. Therefore, for collision avoidance behaviour extraction, route information should not only be regarded as a representation of routine navigation, but also as a behavioural reference for distinguishing expected route-following movement from avoidance-induced manoeuvres.

2.2. Critical encounter extraction

Compared with general route and motion pattern analysis, critical encounter extraction focuses on identifying safety-critical ship-to-ship interactions. Critical encounter extraction has commonly been conducted using two types of criteria: ship-domain-based methods and collision-risk-indicator-based methods. Ship-domain-based methods define a safety area around a ship and identify critical encounters when another ship intrudes into or overlaps with this area (Szlapczynski and Szlapczynska, 2017). Based on this idea, previous studies have used different ship domain models to assess collision risk, detect near-collision events, and support collision-avoidance route planning (Fiskin et al., 2021; Goerlandt et al., 2012; Qu et al., 2011). Another widely used approach is to identify critical encounters through collision risk indicators, such as relative distance, relative speed, Distance to Closest Point of Approach (DCPA), Time to Closest Point of Approach (TCPA), relative bearing, and ship-domain violation. These indicators have been used to monitor collision risk, rank vessel conflicts, identify near-collision scenarios, and map collision-risk hotspots from historical ship trajectories (Mou et al., 2010; Yu et al., 2025; Zhang et al., 2024; Zhang et al., 2015). Chen et al. (2018) developed a Time Discrete Non-linear Velocity Obstacle

(TD-NLVO) method to identify potential collision candidates from historical ship trajectories. Zhao et al. (2026) developed a collision risk assessment framework that preserves high-risk ship interactions in congested waterways and predicts strategic ship responses during encounters. These studies provide useful tools for screening potentially risky ship pairs. However, because criticality is mainly defined by spatial proximity, domain intrusion, or risk thresholds, they do not always verify whether an observable collision avoidance manoeuvre actually occurred.

To capture manoeuvring behaviours, several studies have proposed methods based on observable course alterations. Rong et al. (2022b) employed a sliding window algorithm to identify collision avoidance behaviours by analysing variations of the relative distance, Rate of Turn (ROT), and its derivative in the sliding window. Zhang et al. (2023a) developed a two-stage collision avoidance behaviour extraction algorithm, where the Douglas-Peucker (DP) algorithm was first used to identify steering points, and ROT was then used to detect avoidance behaviours. These studies move beyond risk indicators by incorporating observable manoeuvring behaviour. However, their behaviour detection mainly relies on course alterations in fixed windows. Such designs may not fully capture the complete evolution pattern of collision avoidance behaviour, and short-term course fluctuations may be misidentified as avoidance actions. Although the above studies incorporate manoeuvring behaviours into critical encounter extraction, they mainly focus on detecting course alterations or turning features, while the avoidance intention behind these manoeuvres remains insufficiently explored. Some recent studies have further attempted to interpret collision avoidance intention and ship-to-ship interaction patterns from observed manoeuvring behaviour (Jia et al., 2022; Zhang et al., 2024). These studies provide useful insights into how ships interact during encounter situations. However, their focus remains mainly on describing encounter dynamics, rather than constructing behaviour-based critical encounter scenarios that explain how potential traffic conflicts are actually resolved. In particular, the link between manoeuvring behaviour, avoidance intention, and the specific target ship involved in the interaction remains insufficiently established. Based on the above literature review, Table 1 compares the related studies from four dimensions: ship motion pattern modelling, ship-to-ship interaction extraction, manoeuvring behaviour identification, and avoidance intention analysis. These dimensions represent the main information needed to extract collision avoidance behaviour from ship trajectories. The comparison shows that existing studies have separately addressed regular traffic patterns, risky encounters, manoeuvring changes, and avoidance intention. However, limited attention has been paid to integrating these aspects within a unified framework for the precise extraction of collision avoidance behaviour from ship trajectories in real maritime traffic.

Table 1. Limitations of reviewed literature.

Literature	Ship motion modelling	Ship-to-ship interaction extraction	Manoeuvring behaviour identification	Avoidance intention analysis	Limitations
(Li and Yang, 2023; Rong et al., 2024; Li et al., 2024b)	⚑	⚐	⚐	⚐	Ship route patterns are widely used to support route planning, abnormal behaviour detection, and trajectory prediction. However, the importance of route information in interpreting collision avoidance manoeuvres is overlooked.
(Qu et al., 2011; Goerlandt et al., 2012; Fiskin et al., 2021)	⚐	Δ	⚐	⚐	These ship-domain-based methods identify potentially unsafe or domain-violation situations, but do not verify whether observable collision avoidance manoeuvres actually occurred.
(Mou et al., 2010; Zhang et al., 2015; Chen et al., 2018; Yu et al.,2025; Zhao et al., 2026)	⚐	Δ	⚐	⚐	These risk-indicator-based methods can screen potential conflict states, but criticality is mainly defined by risk thresholds or geometric relationships rather than behaviourally verified avoidance actions.
(Rong et al., 2022b; Zhang et al., 2023a)	⚐	Δ	⚑	⚐	These methods detect manoeuvring behaviours by analysing the course alteration in fixed windows, but may not fully capture the evolution pattern of collision avoidance behaviours and may misidentify short-term fluctuations as avoidance actions.
(Zhang et al., 2024)	⚐	⚑	⚑	Δ	The method links manoeuvring behaviour with avoidance intention, but mainly relies on observed kinematic and angular changes, making the association between the manoeuvre and the actually avoided target ship insufficiently explicit.
(Jia et al., 2022)	⚐	⚑	Δ	Δ	The interaction primitives are learned from neural network-based latent representations and clustering results, so their physical link to explicit collision avoidance intention, avoided target ships, and avoidance strategies remains insufficiently clear.
This study	⚑	⚑	⚑	⚑	The proposed framework integrates route-following baseline modelling, CPD-based manoeuvre detection, and intention-informed target-ship association to extract behaviourally meaningful critical encounter scenarios.

Note: ⚑ indicates that the aspect is explicitly addressed; Δ indicates that the aspect is partially addressed; ⚐ indicates that the aspect is not considered.

2.3. Research gaps

Based on the above review, the following research gaps are identified, highlighting the need for a route-aware and intention-informed framework that can support behaviour-grounded critical encounter extraction for understanding latent traffic conflicts and real-world ship interaction patterns:

Gap 1: From the perspective of the Convention on the International Regulations for Preventing Collisions at Sea (COLREGs) and maritime traffic safety, critical encounter scenarios should reflect ship-to-ship interactions in which navigational responsibilities and avoidance actions are involved. However, many existing encounter extraction methods identify critical scenarios mainly based on collision risk indicators and observed course alterations. Although these methods can identify potentially risky ship pairs, they do not always verify whether ship-to-ship interactions actually occurred. As a result, the extracted scenarios may represent potential geometric conflicts rather than behaviourally verified avoidance interactions, limiting their value for learning collision avoidance strategies and supporting MASS testing.

Gap 2: Existing collision avoidance behaviour identification methods often rely on local kinematic variations, such as course change, ROT, DCPA, or TCPA, within fixed or sliding windows. Such local-window designs may not fully capture the complete deviation–recovery–stabilisation process of collision avoidance behaviour. Moreover, without a planned-route baseline, routine route-following course alterations in structured waterways may be confused with avoidance-induced manoeuvres, reducing the reliability and temporal accuracy of behaviour identification.

Gap 3: Even when a manoeuvring segment is detected, it is not always clear whether the manoeuvre was caused by ship-to-ship avoidance or which surrounding ship was being avoided. Existing methods pay limited attention to the avoidance intention behind the observed trajectory change and the association between the manoeuvre and specific target ships. This limits the ability to construct behaviourally meaningful critical encounter scenarios that reveal not only when a ship manoeuvred, but also why it manoeuvred and which ship interaction was involved.

3. Methodology

The proposed framework consists of three sequential modules, as illustrated in Fig. 1. First, historical AIS data are pre-processed to extract representative ship motion patterns and corresponding route centrelines, which characterise normal route-following behaviour. Second, a behaviour change detection module is developed to identify candidate manoeuvres. A route-aware cost function is constructed to capture the kinematic evolution of motion, and a CPD approach is applied to segment trajectories and detect significant behavioural transitions. Third, an intention-informed method is introduced to extract critical encounter scenarios by comparing observed manoeuvring trajectories with virtual route-following references. This enables the identification of avoided target ships and the inference of navigators' avoidance intent. Detailed descriptions of each module are provided in the following subsections.

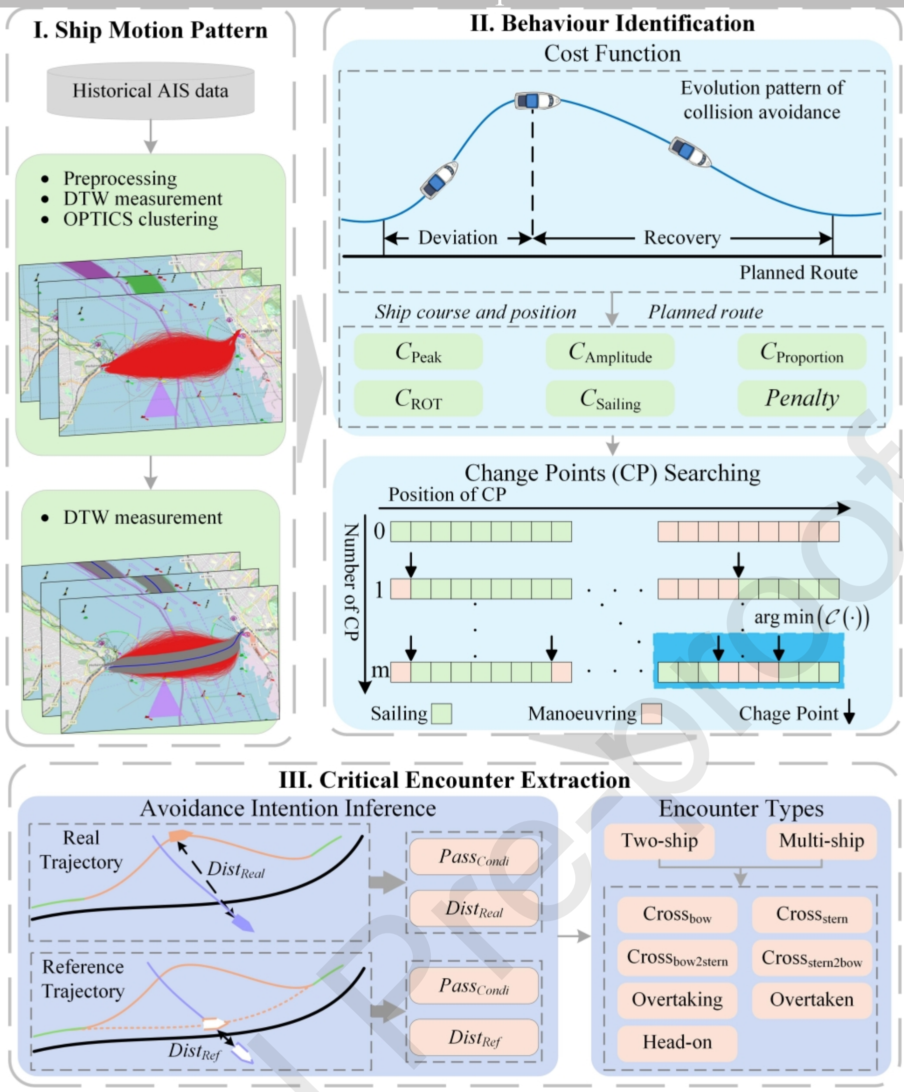

Fig. 1. Research Framework.

3.1. Ship motion pattern

Extracting representative ship motion patterns is essential for understanding the ship routine behaviours. Considering that trajectory clustering is the primary method for revealing underlying motion patterns, a clustering algorithm is employed to group trajectories with similar spatial behaviours into the same cluster (Xin et al., 2025b). Then, the centreline of each trajectory cluster is extracted as the planned route, which represents the spatial distribution of trajectories and serves as the behavioural baseline for subsequent behaviour identification (Rong et al., 2020).

It should be noted that routine behaviours may vary across seasons due to recurrent seasonal changes in navigation environments and operational practices. For example, in high-latitude waters, winter sea ice may restrict navigable areas, concentrate traffic along ice-free channels or icebreaker-assisted fairways, and lead to seasonal deviations from the general traffic centreline. In addition, seasonal changes in traffic demand and operational activities, such as ferry schedules, fishing operations, tourism-related traffic, and port service patterns, may alter the density and composition of traffic flows. Therefore, a single annual centreline may not fully represent normal route-following behaviour under all seasonal conditions. If such season-relative variations are ignored, normal seasonal deviations from the general route may be incorrectly interpreted as deviations from the planned route. Therefore, when evident seasonal route differences exist, the planned route can be constructed as a season-aware route baseline within each trajectory cluster.

3.1.1. Trajectory clustering

Trajectory clustering typically involves two key components: (1) defining an appropriate similarity measure to capture differences among ship trajectories, and (2) selecting a clustering algorithm suited to the considered features. AIS data may contain errors arising from data collection, transmission, or reception errors, as well as temporal asynchronization problems. Pre-processing is necessary before clustering, which includes data filtering, trajectory segmentation, and interpolation to reconstruct complete and reliable trajectories suitable for subsequent analysis (Xin et al., 2025a; Zhang et al., 2021).

(1) Similarity measurement

The ship trajectories are time series of varying lengths, making it challenging to measure their similarity directly using Euclidean distance (Yuan et al., 2017). Distance measurements such as the Hausdorff distance (Wang et al., 2021), Longest Common Subsequence (LCSS) distance (Park et al., 2021), and Dynamic Time Warping (DTW) distance (Li and Yang, 2023), have been widely adopted in trajectory clustering to address this. However, directly computing these distances for all trajectory pairs is inefficient for large-scale AIS datasets. In particular, DTW has a high computational cost when applied to all pairs of trajectories. Moreover, a single spatial distance value may fail to capture voyage-level information, such as origin, destination, and sailing direction. As a result, trajectories with similar spatial locations but different Origin-Destination (OD) pairs may be incorrectly clustered.

To address these limitations, a two-stage clustering strategy is adopted. In the first stage, voyage-level features, including origin, destination, and trajectory length, are used to conduct a first-stage clustering of ship trajectories (Liang et al., 2025; Rong et al., 2024; Zhang et al., 2023b). This stage separates trajectories with different OD characteristics and avoids unnecessary DTW calculations between trajectories that clearly belong to different voyage patterns. In this way, OD information provides an efficient prior for distinguishing major traffic flows and reducing the scale of the subsequent similarity matrix of trajectories.

However, OD-based clustering is insufficient to identify detailed voyage patterns. Trajectories with the same or similar OD pairs may still follow different spatial paths due to Traffic Separation Schemes (TSSs), dredged channels, or local navigation constraints. Therefore, in the second stage, DTW is applied only within each OD-based cluster to measure the detailed spatial similarity between trajectories. This two-stage clustering strategy avoids unnecessary DTW calculations between trajectories with clearly different voyage patterns. It also reduces the risk of incorrectly clustering trajectories that have different but similar OD characteristics, and preserves the ability of DTW to capture detailed trajectory shape similarity.

(2) Clustering algorithm

Clustering algorithms for ship motion pattern extraction can be classified into four categories: distance partition methods (e.g., K-Means (Zhang et al., 2020)), hierarchy methods (e.g., Balanced Iterative Reducing and Clustering using Hierarchies-BIRCH (Yan et al., 2023)), density methods (e.g., Density-Based Spatial Clustering of Applications with Noise-DBSCAN (Zhang et al., 2025)), and spectral clustering (Li and Yang, 2023). Distance partition and hierarchy methods are less suited to AIS trajectory data due to their reliance on convex cluster assumptions and limited ability to handle noise. Spectral clustering is computationally prohibitive for large-scale datasets. Density methods are therefore adopted, as they can handle noise without prior assumptions on cluster number or geometry with rather lower computational complexity.

OPTICS (Ankerst et al., 1999) is selected over DBSCAN as the reachability plot provides a visualisation of the underlying density structure of the trajectory data, upon which an appropriate density threshold is identified for the clustering process. This offers a more transparent and informed basis for parameter selection than the direct threshold specification required by DBSCAN (Rong et al., 2022a). The algorithm is detailed in Appendix A.

3.1.2. Centreline construction

The trajectory clusters are sets of trajectories with high similarity, involving abundant similar trajectory information. Therefore, the centreline of each cluster is extracted to represent the planned route in the cluster (Zhang et al., 2023b). Due to the inconsistency in trajectory lengths within the same cluster, DTW is employed to establish the mapping relationship between trajectories, which can non-linearly warp the path to minimise the distance between trajectories and align them (Li et al., 2022; Rong et al., 2019). The DTW algorithm is detailed in Appendix B. Then, after aligning the trajectories in the same cluster, the centreline is derived from the arithmetic mean of the aligned positions.

3.2. Ship behaviour identification

In this study, ship behaviours are classified into three types: candidate collision avoidance behaviour, collision avoidance behaviour, and route-following behaviour. Their definitions are demonstrated as follows:

Candidate Collision Avoidance Behaviour (CCAB). A trajectory segment exhibiting a distinct deviation-recovery-stabilisation pattern relative to the planned route. Such segments are identified based solely on kinematic characteristics and represent potential collision avoidance actions.

Collision Avoidance Behaviour (CAB). A subset of CCABs for which collision avoidance intention is confirmed. This confirmation is established by identifying one or more target ships that the manoeuvre is intended to avoid.

Route-following Behaviour (RB). A trajectory segment in which the ship continuously follows the planned route, without exhibiting the deviation-recovery-stabilisation collision avoidance pattern.

As aforementioned, most existing ship CAB identification methods focus on variations in kinematic features within fixed time windows. However, CAB is characterised by a clear evolution pattern, typically comprising deviation, recovery, and stabilisation stages, which cannot be fully captured using a predefined temporal scope. Accurate identification of CAB therefore requires an adaptive change detection method that can adaptively adjust the time window to capture this evolution.

CPD provides a framework for identifying structural changes in time series based on pattern differences, without relying on fixed time windows. In transportation research, CPD has been widely adopted to identify behavioural or operational shifts in non-stationary systems. For example, Chen et al. (2022) employed CPD to detect latent structural changes in the evolving spatiotemporal patterns of bike-sharing demand, allowing long-term behavioural regime shifts to be distinguished from short-term fluctuations. Pennetti et al. (2020) utilised CPD to identify critical operational thresholds where highway travel time reliability rapidly degrades, providing a data-driven alternative to fixed capacity assumptions. Bian et al. (2021) used CPD to determine the change points in road systems, mass transit, and micromobility, quantifying policy lead and lag effects across different transportation systems. Cheng et al. (2025) introduced a Bayesian online changepoint detection method to dynamically identify changepoints in traffic flow observation sequences and explain the evolution of traffic state variations, including traffic flow breakdown. These studies demonstrate that CPD is well suited for identifying behavioural change points arising from structural pattern differences, which facilitates its application to the identification of CAB with a distinct evolution pattern.

CPD methods typically consist of three key components: cost function, search method, and constraint. The cost function quantifies the degree of homogeneity within a segment between two consecutive change points, where a lower cost indicates a more consistent pattern and a higher cost suggests the coexistence of multiple patterns. Based on the defined cost function, a search method is employed to determine both the number and locations of change points by minimising the total cost across the entire time series. To prevent over-segmentation, a constraint on the number of change points is introduced.

Fig. 2 illustrates the general workflow of a CPD method. Given an input time series, a search method explores candidate segmentations by varying the number and locations of change points. For each candidate segment, a cost function is computed to quantify within-segment homogeneity. The total cost is obtained by summing the costs of all segments, and the optimal set of change points is determined by minimising the global cost under a predefined constraint.

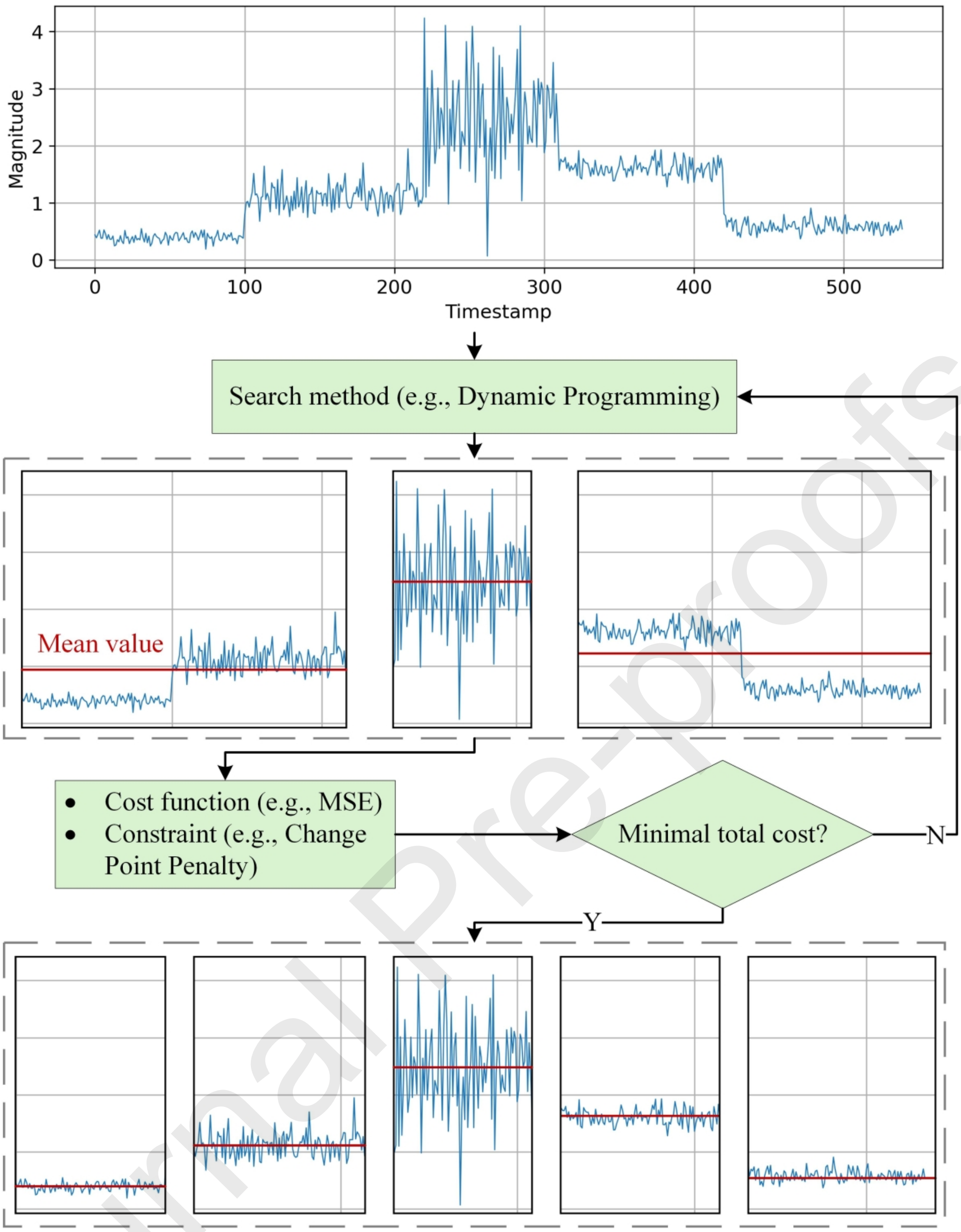

Fig. 2. Workflow of the CPD method.

3.2.1. Cost function

The cost function is the core component of a CPD method, as it quantifies the homogeneity in the evolution pattern within a segment. Ship trajectories may exhibit multiple behavioural modes, including RB and CCAB, which are characterised by distinct evolutionary patterns. To distinguish between these behaviours, behaviour-specific segment cost functions are constructed to capture their respective evolution characteristics. The total cost function is expressed in Eq. (1):

Consider a ship trajectory of length n. Let the set of change points be defined as $0 = k_0 < k_1 < \cdots < k_m < k_{m+1} = n$, where the j^{th} segment is given by $S_j \triangleq \mathcal{T}_{k_j:k_{j+1}}, j = 0,...,m$, and $\mathcal{T}_{a:b}$ denotes the AIS samples from index a to b.

Each segment S_j is associated with a behavioural label $z_j \in \mathcal{B}$, where $\mathcal{B} = \{\text{CCAB,RB}\}$. The total cost is then defined as:

$$F(k,z|\mathcal{T},\mathcal{R}) = \lambda(m)\sum_{j=0}^{m} C_{z_j}\left(S_j,\mathcal{R}_{c_j,\sigma_j}\right) \tag{1}$$

where $C_{\text{CCAB}}(\cdot)$ and $C_{\text{RB}}(\cdot)$ denote the segment cost functions under the CCAB and RB patterns, respectively, $\mathcal{R}_{c_j,\sigma_j}$ denotes the planned route corresponding to S_j, where c_j is the trajectory cluster of S_j and σ_j is the sailing season associated with S_j, $\lambda(m)$ is a penalty term that constrains the number of change points.

The CPD problem is finally formulated as a joint optimisation over change point number and locations, as well as behavioural labels:

$$(k^*,z^*) = \arg\min_{k,z} F(k,z|\mathcal{T},\mathcal{R}) \tag{2}$$

where (k^*,z^*) denote the optimal change point configuration and behaviour labels that minimise the total cost.

Considering that multiple features with different scales and magnitudes are required to characterise the evolution patterns of CCAB and RB, feature normalisation is a necessary pre-processing step. For the distance feature, since the trajectories usually contain a large number of route-following samples and a small number of manoeuvring behaviours with pronounced deviations, using a manually selected threshold may not provide a normalisation with clear physical meaning, especially when the deviation distribution varies across waterways and trajectory clusters. To obtain a data-driven normalisation boundary, a K-means clustering method is applied to the distances between trajectory points and their corresponding planned route points within each trajectory cluster. The number of clusters is set to two, with the aim of separating low-deviation and high-deviation clusters. The low-deviation cluster mainly represents distances that are more consistent with normal route-following behaviour, while the high-deviation regime represents more pronounced deviations from the planned route. Based on the boundary, the distance normalisation is expressed in Eq. (3). In contrast, the course feature is inherently bounded within the range $[-\pi,\pi]$. Therefore, the course relative to planned courses is normalised as Eq. (4).

$$d_i' = \frac{d_i}{KMeans(\mathcal{D}_C)} \tag{3}$$

$$\theta_i' = \frac{\theta_i}{\pi} \tag{4}$$

where d_i' and θ_i' represent the normalised distance and relative course between the i^{th} trajectory point and its corresponding planned route point, $KMeans(\mathcal{D}_C)$ denotes the distance boundary between the two clusters in cluster C and their associated planned route.

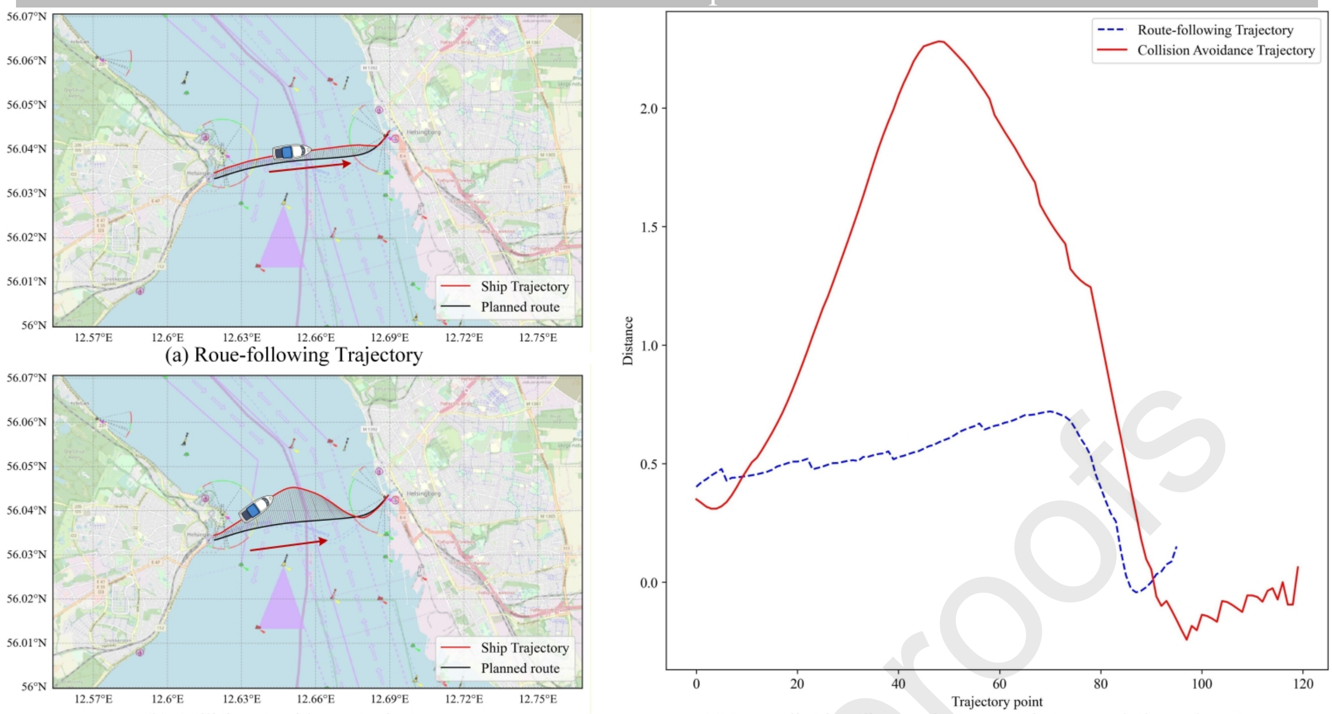

(a) Roue-following Trajectory

(b) Collision Avoidance Trajectory

(c) Normalisation distance between trajectory and planned route

Fig. 3. Illustration of the normalisation method.

Fig. 4 illustrates that a CCAB is composed of three successive stages: deviation, recovery and stabilisation. During deviation, the ship departs from the planned route, leading to an increase in distance. In the recovery stage, counter-turn manoeuvres guide the ship back toward the planned route, and the distance decreases accordingly. After the ship returns to the planned route, course adjustments cause limited fluctuations in distance. Therefore, a CCAB exhibits an increasing–decreasing–fluctuation pattern in the distance relative to the planned route, as shown in Fig. 4(b). The substantial inertia of ships causes a delayed response between course change and the resulting change in relative distance. As a result, the relative course responds earlier and often presents an increasing-decreasing-increasing or decreasing-increasing-decreasing pattern, which corresponds to the deviation, recovery and stabilisation stages.

Although these patterns are monotonic under ideal conditions, in practice, limited ship manoeuvrability introduces oscillations to these evolution patterns. To obtain stable representations, isotonic regression is used to fit a monotonic sequence that corresponds to the CCABs, as expressed in Eq. (5).

$$\begin{cases} \hat{y} = \arg\min\limits_{\hat{y}_i} \sum_{i=1}^{n} (\hat{y}_i - y_i)^2 \\ \text{s.t.} \qquad \hat{y}_1 \le \hat{y}_2 \le \dots \le \hat{y}_n \end{cases} \tag{5}$$

where y_i is the original data, $\hat{y}_i$ represents the isotonic regression value.

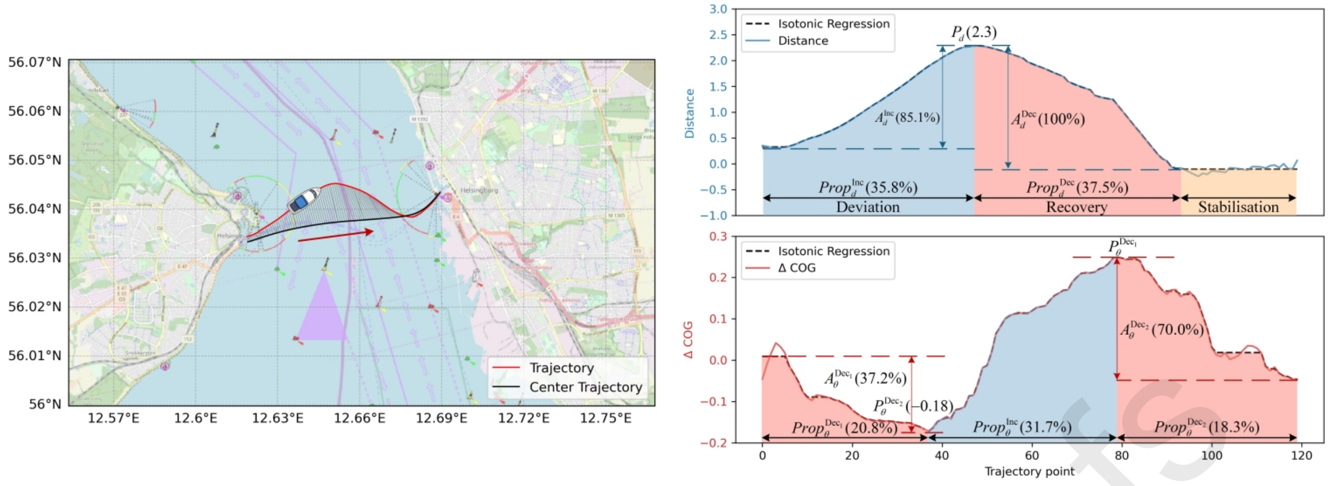

(a) Ship trajectory contains CCAB

(b) Evolution of distance and relative course in CCAB

Fig. 4. Kinematic evolution in CCAB.

To capture these evolutionary characteristics, the cost function components are designed to reflect the kinematic patterns specific to each stage in CCAB, as summarised in Table 2. Based on these components, the $C_{\mathrm{CCAB}}(\cdot)$ in Eq. (1) is expressed in Eq. (6) to jointly evaluate the evolution of relative distance and course deviation throughout the CCAB.

Table 2. Components of the cost function and their roles in CCAB identification

Component	Role
C_x^{Peak}	Characterises the peak magnitude of kinematic feature variations during the deviation and recovery stages, ensuring that CCABs involve sufficient deviation from the planned route.
C_x^{Amp}	Quantifies the amplitude of kinematic feature variations in the deviation and recovery stages, enforcing significant kinematic variations.
C_x^{Prop}	Measures the proportion of kinematic variations within the deviation and recovery stages, ensuring that CCABs exhibit a high density of kinematic changes.
C_θ^{ROT}	Represents the mean absolute ROT within a trajectory segment, capturing substantial course changes during deviation and recovery stages.
$g(\cdot)$	Penalises sailing behaviour to prevent RBs from being misidentified as the stabilisation stage of CCABs.

$$\begin{cases} C_{\mathrm{CCAB}}(S,\mathcal{R}) = C_d + C_\theta \\ C_d = C_d^{Peak} + C_d^{Amp} + C_d^{Prop} + g(S,\mathcal{R}) \\ C_\theta = C_\theta^{Peak} + C_\theta^{Amp} + C_\theta^{Prop} + C_\theta^{ROT} \end{cases} \tag{6}$$

where $C_{\mathrm{CCAB}}(\cdot)$ denotes the cost function for CCAB, C_d and C_θ represent the cost in relative distance and course, $g(\cdot)$ denotes the penalty for RB, C_d^{Peak}, C_d^{Amp}, C_d^{Prop}, C_θ^{Peak}, C_θ^{Amp}, C_θ^{Prop}, and C_θ^{ROT} represent the cost of kinematic features.

The individual components of the CCAB cost function in Eq. (6) are detailed below, with each term designed to capture a specific aspect of the CCABs.

(1) Peak cost

According to Rule 8 of the COLREGs, CABs should be large enough to be readily apparent to other ships. In the trajectory level, this requirement can be reflected by the magnitude of deviation from the planned route. Therefore, the peak values of distance and course relative to the planned route are incorporated into the cost function to characterise the magnitude of CCABs.

Unlike the distance, the relative course evolution in a CCAB typically exhibits two peaks, corresponding to the manoeuvres during the deviation and recovery stages, as illustrated in Fig. 4. To ensure that noticeable course changes can be observed in both stages, the smaller of the two peak values is adopted in the peak cost, as defined in Eqs. (7)-(10).

$$\begin{cases} \mathcal{T}=\{p_1,p_2...,p_n\},\ p_i=(time_i,lon_i,lat_i,COG_i,ROT_i) \\ \mathcal{R}=\{p_1,p_2...,p_m\},\ p_j=\left(lon_j,lat_j,COG_j\right) \\ d=\left\{h\left(lon_i,lat_i,lon_{j(i)},lat_{j(i)}\right)\middle|p_i\in\mathcal{T},p_{j(i)}\in\mathcal{R}\right\} \\ \theta=\left\{\left(COG_i-COG_{j(i)}\right)\middle|p_i\in\mathcal{T},p_{j(i)}\in\mathcal{R}\right\} \\ \hat{d}=ISO(d),\hat{\theta}=ISO(\theta) \end{cases} \tag{7}$$

where $\hat{d}$ and $\hat{\theta}$ indicate the fitted relative distance and course sequence by isotonic regression $ISO(\cdot)$, d and θ are the set of distances and relative course between the trajectory points p_i and their corresponding points $p_{j(i)}$ on the planned route, $\mathcal{T}$ and $\mathcal{R}$ represent the trajectory and the planned route, respectively, $h(\cdot)$ is the Haversine distance calculation function.

$$h\left(lon_i,lat_i,lon_{j(i)},lat_{j(i)}\right)=2R_e\sin^{-1}\left(\sqrt{\begin{matrix}\sin^2\left(\dfrac{lat_i-lat_{j(i)}}{2}\right)+ \\ \cos lat_i\cos lat_{j(i)}\sin^2\left(\dfrac{lon_i-lon_{j(i)}}{2}\right)\end{matrix}}\right) \tag{8}$$

where R_e is the radius of Earth.

$$f_H(a,\tau)=\begin{cases}\dfrac{1}{a+\varepsilon}, & 0\le a\le\tau \\ 0, & a>\tau\end{cases} \tag{9}$$

where $f_H(\cdot)$ denotes the inverse hinge function, τ represents the threshold, ε is a small positive constant.

$$\begin{cases} C_{\mathcal{X}}^{\text{Peak}}=f_H\left(P_{\mathcal{X}},\tau_{\mathcal{X}}^{\text{Peak}}\right),\ \mathcal{X}\in\{d,\theta\} \\ P_{\mathcal{X}}=\min\limits_{s\in S_{\mathcal{X}}}\max(|\hat{\eta}_{\mathcal{X}}^{s}|) \\ S_\theta=\{\text{Dec}_1,\text{Dec}_2\},S_d=\{\text{Inc},\text{Dec}\} \end{cases} \tag{10}$$

where $C_{\mathcal{X}}^{\text{Peak}}$ represents the peak cost associated with feature $\mathcal{X}$, $P_{\mathcal{X}}$ denotes the minimum peak of feature $\mathcal{X}$ across $S_{\mathcal{X}}$, $S_{\mathcal{X}}$ represents the key CCAB patterns, $\hat{\eta}_{\mathcal{X}}^{s}$ denotes the fitted kinematic sequence of feature $\mathcal{X}$ within stage s by isotonic regression, Dec_1 and Dec_2 represent the first and second decreasing patterns in relative course, Inc and Dec denote the increasing and decreasing patterns in relative distance.

(2) Amplitude cost

Due to navigational constraints and restricted waterways, ships may sail approximately parallel to their planned routes. In such situations, the trajectory can exhibit a large deviation from the planned route while involving only limited variation during the approach to the peak. To distinguish CCABs from this type of RBs, an amplitude cost is introduced to characterise the magnitude of variation leading to the peak deviation, as defined in Eq. (11).

$$\begin{cases} C_{\mathcal{X}}^{\text{Amp}} = f_H\left(A_{\mathcal{X}}, \tau_{\mathcal{X}}^{\text{Amp}}\right), \mathcal{X} \in \{d, \theta\} \\ A_{\mathcal{X}} = \dfrac{1}{N_{\mathcal{X}}} \min_{s \in S_{\mathcal{X}}} A_{\mathcal{X}}^{s} \\ A_{\mathcal{X}}^{s} = Range(\hat{\eta}_{\mathcal{X}}^{s}), N_{\mathcal{X}} = Range(\hat{\eta}_{\mathcal{X}}) \\ Range(x) = \max(x) - \min(x) \\ S_{\theta} = \{\text{Dec}_1, \text{Dec}_2\}, S_d = \{\text{Inc}, \text{Dec}\} \end{cases} \tag{11}$$

where $C_{\mathcal{X}}^{\text{Amp}}$ represents the amplitude cost associated with feature $\mathcal{X}$, $A_{\mathcal{X}}$ denotes the minimum normalised amplitude of feature $\mathcal{X}$ across $S_{\mathcal{X}}$, $A_{\mathcal{X}}^{s}$ represents the amplitude of feature $\mathcal{X}$ in s, $N_{\mathcal{X}}$ denotes the overall amplitude of feature $\mathcal{X}$, serving as a normalisation factor.

(3) Proportion cost

In contrast to RBs, which generally follow the planned route, CCAB exhibits distinct deviation and recovery stages. Therefore, the proportion of kinematic features' variations in CCABs is expected to be much higher than this in RBs. Based on this difference, a proportion cost is introduced to quantify the proportion of kinematic variations during the deviation and recovery stages, as defined in Eq. (12).

$$\begin{cases} C_{\mathcal{X}}^{\text{Prop}} = f_H\left(Prop_{\mathcal{X}}, \tau_{\mathcal{X}}^{\text{Prop}}\right), \mathcal{X} \in \{d, \theta\} \\ Prop_{\mathcal{X}} = \dfrac{1}{n_s - 1} \min_{s \in S_{\mathcal{X}}} \sum_{k=1}^{n_s - 1} I\left(\hat{\eta}_{\mathcal{X},k}^{s}, \hat{\eta}_{\mathcal{X},k+1}^{s}\right) \\ I(a, b) = \begin{cases} 0, a = b \\ 1, a \neq b \end{cases} \\ S_{\theta} = \{\text{Inc}, \text{Dec}\}, S_d = \{\text{Inc}, \text{Dec}\} \end{cases} \tag{12}$$

where $C_{\mathcal{X}}^{\text{Prop}}$ represents the proportion cost associated with feature $\mathcal{X}$, $Prop_{\mathcal{X}}$ denotes the minimum proportion of variation of feature $\mathcal{X}$ across $S_{\mathcal{X}}$, $\hat{\eta}_{\mathcal{X},k}^{s}$ represents the k^{th} fitted kinematic sequence of feature $\mathcal{X}$ during s by isotonic regression, n_s denotes the number of elements in s, $I(\cdot)$ denotes the indicator function, the Dec in S_{θ} is constructed by concatenating the fitted sequences of Dec_1 and Dec_2.

(4) ROT cost

The Rate of Turn (ROT) reflects the rate of change in ship course. Given that COLREGs require the ship to avoid a succession of small alterations of course in collision avoidance, the average of ROT is introduced to capture the course variations. Consequently, the ROT cost is defined as Eq. (13).

$$\begin{cases} C_{\theta}^{\text{ROT}} = f_H\left(\overline{ROT}, \tau_{ROT}\right) \\ \overline{ROT} = \dfrac{\sum_{j=2}^{n} |ROT_j|}{n - 1} \\ ROT_j = \dfrac{COG_j - COG_{j-1}}{time_j - time_{j-1}} \end{cases} \tag{13}$$

where $\overline{ROT}$ denotes the average of $|ROT|$, ROT_j represents the j^{th} point in ROT.

(5) RB Penalty

According to the evolution pattern, a CCAB consists of three successive stages: deviation, recovery, and stabilisation. The stabilisation stage occurs after the ship has returned to the planned route. It remains part of the collision avoidance process, as the ship still needs to adjust course to the planned course due to manoeuvring inertia. As a result, stabilisation and RB may exhibit similar patterns. To prevent RBs from being misidentified as the stabilisation stage of CCABs, an RB penalty function is introduced. This penalty is based on the fact that RBs often occur only before or after a CCAB, rather than within it, and therefore focuses on the variation trends of kinematic features outside the CCAB evolution pattern. The RB penalty is shown in Eq. (14).

$$g(S,\mathcal{R}) = \sum_{j=1}^{0.2n-1} f_H\left(\hat{d}_{j+1} - \hat{d}_j, 0\right) + \sum_{j=0.8n}^{n-1} f_H\left(\hat{d}_{j+1} - \hat{d}_j, 0\right) \tag{14}$$

where $g(\cdot)$ denotes the RB penalty.

This method aims to identify CCABs by evaluating the consistency of each trajectory segment with both CCAB and RB patterns. Specifically, the CCAB cost function quantifies the similarity between the kinematic variation patterns within a trajectory segment and the characteristic evolution of CCABs, while an RB cost function is introduced to characterise route-following behaviour. Unlike CCABs, which exhibit clear deviation and recovery stages, RBs are characterised by motion that follows the planned route, resulting in limited variations in both relative distance and course. Accordingly, the RB cost function is defined in Eq. (15) to yield low cost for trajectory segments that exhibit route-following characteristics:

$$C_{\mathrm{RB}}(S,\mathcal{R}) = \sum\nolimits_{i=1}^{n} \left(|\hat{d}_i| + |\hat{c}_i|\right) \tag{15}$$

where $C_{\mathrm{RB}}(\cdot)$ represents the RB cost function.

3.2.2. Constraints

To prevent the number of change points from increasing indefinitely, a change point penalty $\lambda(m)$ is introduced to regularise segmentation complexity. Unlike additive penalties that are imposed as a fixed constant, this study employs a multiplicative penalty factor that affects the total segmentation cost, as shown in Eq. (1). As the number of change points increases, the penalty increases accordingly, which effectively prevents over-segmentation. Compared with a fixed penalty, this formulation reduces sensitivity to the penalty magnitude and enables more robust identification of the optimal segmentation. The change point penalty is expressed as Eq. (16).

$$\lambda(m) = m(1 + \tau_{Decline}) \tag{16}$$

where $\lambda(m)$ denotes the change point penalty, m is the number of change points, $\tau_{Decline}$ represents the threshold of the expected decline proportion in total cost when increasing one change point.

3.2.3. Search method

The Dynamic Programming (DP) is a popular optimal detection algorithm for searching for change points, yielding exact solutions (Truong et al., 2020). Compared to the exhaustive search, which has the time complexity of $O(C_n^k)$, the DP algorithm significantly reduces the time complexity to $O(kn^2)$. The algorithm is summarised as follows:

(1) **Data preparation (Lines 1-4):** Given that the warping path generated by DTW enables a flexible, non-linear alignment between the two trajectories (Li et al., 2020), DTW is employed to extract the relative distance $\mathcal{D}$ and course $\theta^{\mathcal{M}}$ for each trajectory point with respect to the centreline. Then, the relative distance and course are normalised to mitigate the influence of different dimensions by Eqs. (3) and (4).

(2) **Dynamic programming (Lines 5-18):** First, calculate the minimal cost and corresponding ship behaviour in each subsegment (u,v). Then, the DP algorithm is utilised to establish the dynamic programming table $\mathcal{F}[m,t]$ and the backtrack table $\mathcal{L}[m,t]$, which represent the minimal cost from the first trajectory point to the t^{th} point under m change points, and the corresponding position of change points, respectively.

(3) **Backtrack (Lines 19-33):** According to the backtrack table $\mathcal{L}[m,t]$, which records the index of each change point, the optimal change point $\mathcal{K}$ under m^* is identified according to the backtrack table.

The pseudocode of the proposed ship behaviour identification algorithm is illustrated in Algorithm 1.

Algorithm 1. Identification of ship CCABs.

Input: $\mathcal{T}=\{p_1,p_2...,p_n\}$, $p_i=(lon_i,lat_i,COG_i,ROT_i)$, $\mathcal{R}=\{r_1,r_2...,r_q\}$, $r_j=\left(lon_j,lat_j,COG_j\right)$ // $\mathcal{T}$ *and* $\mathcal{R}$ *denote the trajectory of own ship and the planned route, respectively*;

Output: $\mathcal{K}=\{k_1,k_2,\cdots,k_m|0=k_0<k_1<...<k_{m+1}=n\}\ or\ \{\phi\}$ // $\mathcal{K}$ represents a set of behavioural change points in $\mathcal{T}$;

Procedure:

1. Ship motion patterns extraction.
2. $[\mathcal{M},\mathcal{D}]\leftarrow DTW(\mathcal{T},\mathcal{R})$; // Function DTW is defined in Eqs. (B.1) and (B.2).
3. $\theta_i^{\mathcal{M}}\leftarrow COG_i^T-COG_{j(i)}^R$; // $j(i)$ represents index of $\mathcal{R}$ mapped to the COG_i^T under *DTW* mapping $\mathcal{M}$.
4. $[\mathcal{D}',\theta']\leftarrow Norm(\mathcal{D},\theta^{\mathcal{M}})$; // Function $Norm$ is defined in Eqs. (3) and (4).
5. ***for all*** $(u,v),1\le u<v\le n$ ***do***:
6. $\quad\mathcal{C}(u,v)\leftarrow\min_{z\in B}C_z(\mathcal{S}_{u:v}(\mathcal{T},\mathcal{R}))$,$\mathcal{B}=\{\text{CCAB,RB}\}$;
7. $\quad\mathcal{B}(u,v)\leftarrow\arg\min_{z\in B}C_z(\mathcal{S}_{u:v}(\mathcal{T},\mathcal{R}))$,$\mathcal{B}=\{\text{CCAB,RB}\}$;
8. ***end for***
9. ***Initialise*** $\mathcal{F}[0{:}K_{Max},0{:}n]\leftarrow\infty,\mathcal{L}[0{:}K_{Max},0{:}n]\leftarrow-1$;
10. ***for*** $t=1\ to\ n$ ***do***:
11. $\quad\mathcal{F}[0,t]=\mathcal{C}(0,t)$;

---

end for

for $m = 1$ to K_{Max} ***do***: // K_{Max} is a parameter, denoting the maximal number of change points.

  for all $t,s \in \{1,2,\ldots,n\}, s < t$ ***do***:

    $\mathcal{F}[m,t] \leftarrow \min(\mathcal{F}[m-1,s] + \mathcal{C}(s,t))$;

    $\mathcal{L}[m,t] \leftarrow \arg\min_{s}(\mathcal{F}[m-1,s] + \mathcal{C}(s,t))$;

  end for

end for

initialise $m^* \leftarrow 0$;

for $m = 1$ to K_{Max} ***do***:

  if $\mathcal{F}[m,n] < \mathcal{F}[m^*,n]$:

    $m^* \leftarrow m$;

  end if

end for

set $\mathcal{K} \leftarrow []$;

while $m^* > 0$:

  $l \leftarrow \mathcal{L}[m^*,n]$;

  append l ***to*** $\mathcal{K}$;

  $t \leftarrow l$;

  $m^* \leftarrow m^* - 1$;

end while

$\mathcal{K} \leftarrow \mathrm{reverse}(\mathcal{K})$;

return $\mathcal{K}$;

3.2.4. Parameter Calibration

Since the cost function and constraints involve multiple threshold parameters that interact jointly, determining appropriate values through domain knowledge alone is infeasible. To address this, a three-step parameter calibration procedure is adopted.

(1) **Sample annotation:** a random sample of trajectories is manually annotated by maritime experts as either CCAB or route-following behaviour, yielding a labelled dataset for threshold evaluation.

(2) **Parameter space compression:** Each parameter is first discretised into a finite set of candidate values based on domain knowledge, reducing the search from a high-dimensional continuous space to a multi-dimensional discrete space. Since the number of possible combinations grows exponentially with the number of parameters, exhaustive grid search remains computationally prohibitive. Compared with random search (Bergstra et al., 2011) and Bayesian optimisation (Snoek et al., 2012), the orthogonal experimental design (Taguchi, 1987) can significantly save the tuning time while preserving satisfactory performance (Zhang et al., 2019). An orthogonal experimental design is therefore employed to systematically sample a representative subset of combinations.

(3) **Performance evaluation:** Each parameter combination is evaluated on the labelled dataset using accuracy, precision, recall, and F1-score. The parameter set with the best overall performance is selected as the final threshold configuration.

3.3. Ship encounter extraction

While the CCABs have been identified in the previous section, it is essential to note that CCABs can arise not only from two-ship or multi-ship encounters, but also from environmental influences and human operational limitations. To accurately identify the CABs and the corresponding encounter scenarios, an intention-informed critical encounter extraction method is proposed. The core of this method lies in comparing the real trajectory with the possible route-following trajectory to investigate the reason for taking manoeuvring actions, thereby inferring the avoidance intention and extracting critical encounters. Consequently, a reference trajectory is proposed, which is a virtual trajectory that follows the planned route without manoeuvring action, as illustrated in Fig. 5. By comparing the ship interactions in the real and reference trajectories, critical encounter situations are categorised into eight representative types. The detailed procedure is presented in Algorithm 2.

Algorithm 2. Intention-informed critical encounter extraction algorithm.

Input: $\mathcal{T}=\{p_1,p_2\dots,p_n\}$, $\mathcal{T}^{(s)}=\left\{p_1^{(s)},p_2^{(s)},\dots,p_{ns}^{(s)}\right\}$, $\mathcal{T}_{sur}=\{\mathcal{T}^{(s)}|s=1,2,\dots,L\}$, $\mathcal{R}=\{r_1,r_2,\dots,r_q\}$, $p_i=(time_i,lon_i,lat_i,COG_i,SOG_i,ROT_i,status_i)$, $status_i\in\{\text{CCAB},\text{RB}\}$, $r_j=\left(time_j,lon_j,lat_j,COG_j\right)$;

Output: $\mathcal{E}=\left\{\left(t_s,t_e,\mathcal{T},\mathcal{T}^{(s)},type\right)|s\in\mathcal{S}\right\}$ // $\mathcal{E}$ represents the critical encounters between $\mathcal{T}$ and $\mathcal{T}_{sur}$, $\mathcal{S}$ denotes the set of $\mathcal{T}_{sur}$ that constitute critical encounter with $\mathcal{T}$.

Procedure:

Data pre-processing.

$[\mathcal{M},\mathcal{D}]\leftarrow DTW(\mathcal{T},\mathcal{R})$; // Function DTW is defined in Eqs. (B.1) and (B.2).

$\mathcal{T}_{CCAB}=\{p_i|p_i(status_i)=\text{CCAB}\}$; // $\mathcal{T}_{CCAB}$ denotes the CCAB in $\mathcal{T}$.

$\mathcal{R}_{CCAB}^{\mathcal{M}}=\left\{p_{j(i)}|p_i(status_i)=\text{CCAB}\right\}$; // $\mathcal{R}_{CCAB}^{\mathcal{M}}$ represents the corresponding planned route under DTW mapping $\mathcal{M}$.

$\mathcal{T}_{Ref}\leftarrow RefGen\left(\mathcal{T}_{CCAB},\mathcal{R}_{CCAB}^{\mathcal{M}}\right)$; // $\mathcal{T}_{Ref}$ denotes the reference trajectory, which is assumed to maintain the course of the planned route, as illustrated in Fig. 5.

$\mathcal{E}\leftarrow\{\}$;

for s in $1,2,\cdots,L$ ***do***:

    Determine the encounter type $E\in\{\text{Head- on},\text{Crossing},\text{Overtaking},\text{Overtaken}\}$, following COLREGs.

    Calculate the condition and distance when $\mathcal{T}_{\mathrm{X}}$ passed $\mathcal{T}^{(s)}$, $\mathrm{X}\in\{\text{CCAB},\text{Ref}\}$; // $\left[PassCond_X^{(s)},PassDis_X^{(s)}\right]$, $PassCond_X^{(s)}\in\{\text{bow},\text{stern},\text{None}\}$.

    if $PassCond_X^{(s)}=None$:

        break

    else:

The critical encounters and the corresponding types $type$ are determined by comparing $PassCond_X^{(s)}$ and $PassDis_X^{(s)}$ in real trajectory and reference trajectory, as shown in Fig. 5.

$T \leftarrow \{time_i | p_i \in \mathcal{T}\}$, $T^{(s)} \leftarrow \left\{time_j^{(s)} | p_j^{(s)} \in \mathcal{T}^{(s)}\right\}$, $[t_s, t_e] \leftarrow \left[\min(T \cap T^{(s)}), \max(T \cap T^{(s)})\right]$;

add $\left(t_s, t_e, \mathcal{T}, \mathcal{T}^{(s)}, type\right)$ ***to*** $\mathcal{E}$;

| ***end if***

end for

return $\mathcal{E}$;

To accurately extract critical encounter scenarios, the reference trajectory is defined as a baseline to identify involved ships and corresponding encounter types by analysing the characteristics of the eight encounter categories illustrated in Fig. 5 and the definitions of intention-informed encounter types are summarised in Table 3. The algorithm is summarised as follows:

(1) **Reference trajectory**: To distinguish ships involved in critical encounters from those with negligible impact, the reference trajectory is constructed to represent a virtual trajectory under the assumption of sailing along the planned course with no CCAB. This reference trajectory serves as a behavioural baseline, reflecting the navigation intention of following the planned course without external disturbance. By comparing the reference trajectory with the real trajectory involving CCABs, the differences in interaction with surrounding ships caused by CCABs can be revealed, thereby determining CAB and critical encounter scenarios. The formulation of generating reference trajectory $RefGen\left(\mathcal{T}_{CCAB}, \mathcal{R}_{CCAB}^{\mathcal{M}}\right)$ is expressed in Eq. (17).

$$\begin{cases} \mathcal{T}_{Ref} = \left\{p_1^{Ref}, p_2^{Ref} \dots, p_q^{Ref}\right\}, p_i^{Ref} = \left(time_i^{Ref}, SOG_i^{Ref}, lon_i^{Ref}, lat_i^{Ref}, COG_i^{Ref}\right) \\ time_i^{Ref} = \{p_i(time_i) | p_i \in \mathcal{T}_{CCAB}\} \\ SOG_i^{Ref} = \{p_i(SOG_i) | p_i \in \mathcal{T}_{CCAB}\} \\ COG_i^{Ref} = \left\{r_j(COG_j) | r_j(time_j) \in time_i^{Ref}\right\} \\ lon_i^{Ref} = lon_{i-1}^{Ref} + \dfrac{SOG_i^{Ref} \cdot \sin(COG_i^{Ref})}{(time_i^{Ref} - time_{i-1}^{Ref})} \\ lat_i^{Ref} = lat_{i-1}^{Ref} + \dfrac{SOG_i^{Ref} \cdot \cos(COG_i^{Ref})}{(time_i^{Ref} - time_{i-1}^{Ref})} \end{cases} \tag{17}$$

where $\mathcal{T}_{Ref}$ represents the reference trajectory, p_i^{Ref} denotes the i^{th} point in $\mathcal{T}_{Ref}$.

(2) **Avoidance intention**: The avoidance intention characterises the underlying strategy behind a collision avoidance manoeuvre, and a similar CCAB may correspond to different intentions. By comparing the relative positions between ships in the real manoeuvring trajectory and the reference trajectory, four distinct intention types in crossing encounters are identified, as illustrated in Figs. 5(a)-(d). Based on the avoidance intention, critical encounters can be extracted effectively, thereby improving the method's interpretability.

(3) **Data preparation**: In addition to the DTW mapping $\mathcal{M}$ and the distance $\mathcal{D}$ between trajectory points, three key trajectories are determined in data preparation: the ship manoeuvring trajectory

$\mathcal{T}_{CCAB}$, the corresponding planned route $\mathcal{R}_{CCAB}^{\mathcal{M}}$, and the reference trajectory $\mathcal{T}_{Ref}$. For each surrounding ship, the passing condition $PassCond \in \{\text{bow,stern,None}\}$ and the passing distance $PassDist$ when ships pass each other are calculated to serve as the encounter characteristic.

(4) **Crossing encounter extraction**: Crossing is one of the most common and complex encounter types. Although COLREGs state that *"avoid crossing ahead of the other vessel"*, such behaviour is still frequent, especially in multi-ship encounter scenarios. Through comparing the $PassCond$ of reference trajectory and the actual trajectory, the crossing encounter scenarios can be divided into four patterns: stern-to-stern, bow-to-bow, bow-to-stern, and stern-to-bow, illustrated in Figs. 5(a)-(d). Obviously, the bow-to-stern and stern-to-bow patterns exhibit a significant change in $PassCond$ and can be extracted as the critical encounters. However, for the stern-to-stern and bow-to-bow patterns, to filter out the conditions that the ships pass at a long distance showing negligible impact, the threshold of distance τ_{Dis} is introduced to ensure that the CAB results in a significant increase in passing distance.

(5) **Overtaking and overtaken encounter extraction**: According to Rule 13 of COLREGs, *"any vessel overtaking any other shall keep out of the way of the vessel being overtaken"* and *"when a ship is approaching another ship from a direction more than 22.5° abaft the beam, the encounter is classified as an overtaking scenario."* Therefore, an overtaking scenario should satisfy the following two necessary conditions: (1) the own ship takes an evasive action; and (2) when the action is taken, the own ship is in a direction more than 22.5° abaft the beam of the target ship, and after the avoidance action is completed, the own ship is located ahead of the target ship. Under this condition, overtaking and overtaken encounters can be identified based on the relative bearing at the start and end of the CCAB, as illustrated in Figs. 5(e) and (f).

(6) **Head-on encounter extraction**: Unlike crossing and overtaking encounters, a head-on encounter involves two ships approaching each other on reciprocal or nearly reciprocal courses. According to the COLREGs, both ships are expected to take evasive actions, normally by altering course to starboard and passing port-to-port. However, in real navigation, the evasive action may also be affected by environmental constraints. Therefore, in this study, a head-on critical encounter is identified when the reciprocal or nearly reciprocal approaching condition is satisfied, and CABs are observed for both ships, as illustrated in Fig. 5(g).

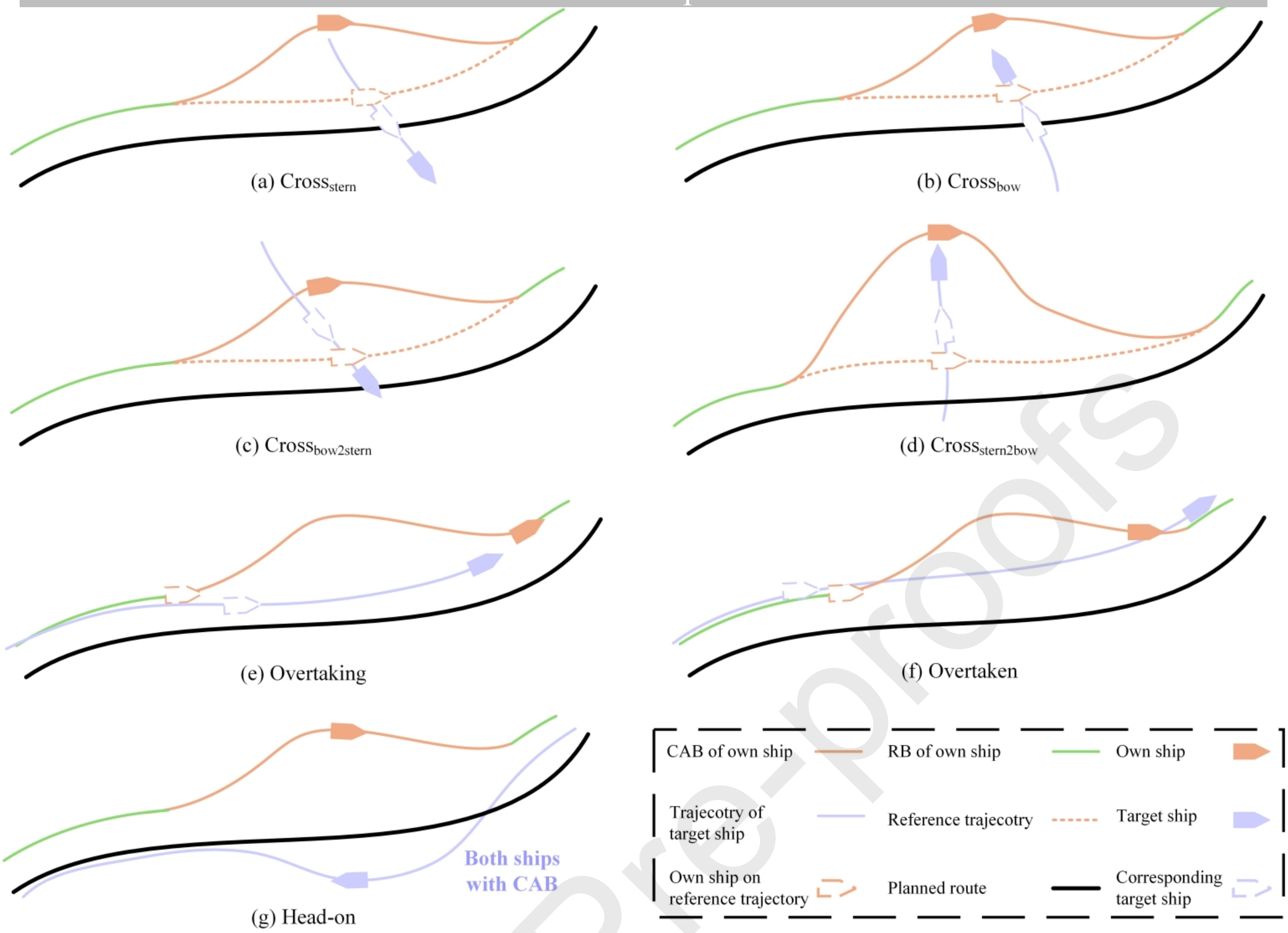

Fig. 5. Diagram of critical encounter extraction.

Table 3. Definitions of intention-informed encounter types.

Encounter Types	Definition
Head-on	A head-on encounter in which **both ships exhibit identified CABs** and during the interaction these two ships meet on reciprocal or nearly reciprocal courses.
$Cross_{bow}$	A crossing encounter in which both the reference and observed trajectories **pass ahead of the target ship**, and the observed trajectory increases the passing distance relative to the reference trajectory by at least τ_{Dis}.
$Cross_{bow2stern}$	A crossing encounter in which the passing condition changes **from passing ahead** in the reference trajectory **to passing astern** in the observed trajectory.
$Cross_{stern}$	A crossing encounter in which both the reference and observed trajectories **pass astern of the target ship** and the observed trajectory increases the passing distance relative to the reference trajectory by at least τ_{Dis}.
$Cross_{stern2bow}$	A crossing encounter in which the passing condition changes **from passing astern** in the reference trajectory **to passing ahead** in the observed trajectory.
Overtaking	An encounter in which own ship approaches target ship from a relative bearing exceeding 22.5° abaft the **target ship's beam** and subsequently passes ahead of the target ship.
Overtaken	An encounter in which target ship approaches own ship from a relative bearing exceeding 22.5° abaft the **own ship's beam** and subsequently passes ahead of the own ship.

Note: In all aforementioned encounter types, the own ship exhibits identified CABs.

To evaluate the effectiveness of the proposed framework, the validation in this study is conducted at three levels. First, standard encounter scenarios are used to examine whether the method can correctly detect collision avoidance behaviour under typical navigational situations. Second, representative real-world AIS cases are employed to assess the practical applicability of the framework in realistic traffic environments. Third, the extracted encounter scenarios are further analysed for behavioural consistency and criticality representation to verify whether the proposed method can not only reliably identify avoidance manoeuvres but also support the extraction of meaningful critical encounter scenarios. Through this multi-level validation design, the performance of the proposed framework is examined from the perspectives of detection capability, practical applicability, and scenario extraction effectiveness.

4. Case study

4.1. Research area and data pre-processing

To demonstrate the proposed framework, the Øresund is selected as the research area, which involves the HH ferry route (Helsingør–Helsingborg) connecting Helsingør, Denmark and Helsingborg, Sweden. As one of the busiest ferry routes in the world, the HH ferry route intersects with three lateral traffic flows (Fig. 6), resulting in a high frequency of ship collision avoidance behaviours.

The research area spans from 56°N to 56.07°N latitude and from 12.55°E to 12.77°E longitude. The AIS data used in this paper are collected from January 1, 2024, to December 31, 2024, and contain over 61 million records. Each AIS record contains details such as time, Maritime Mobile Service Identity (MMSI) number, latitude, longitude, Speed Over Ground (SOG), Course Over Ground (COG), ship length, and ship type. Prior to analysis, a three-step pre-processing procedure is applied to eliminate errors and ensure data quality. First, trajectories are segmented using a time interval threshold of 900 s (Liu et al., 2024; Wang et al., 2022). Second, segments crossing land are removed, as such patterns indicate errors arising from data transmission or reception faults (Zhao et al., 2018). Third, linear interpolation at a time interval of 10 s is applied to each segment to standardise the varying message transmission frequencies across different ships (Xin et al., 2024). Through the pre-processing, the 8503 raw trajectories are reduced to 44530 validated segments across 7799 ships, as illustrated in Fig. 6.

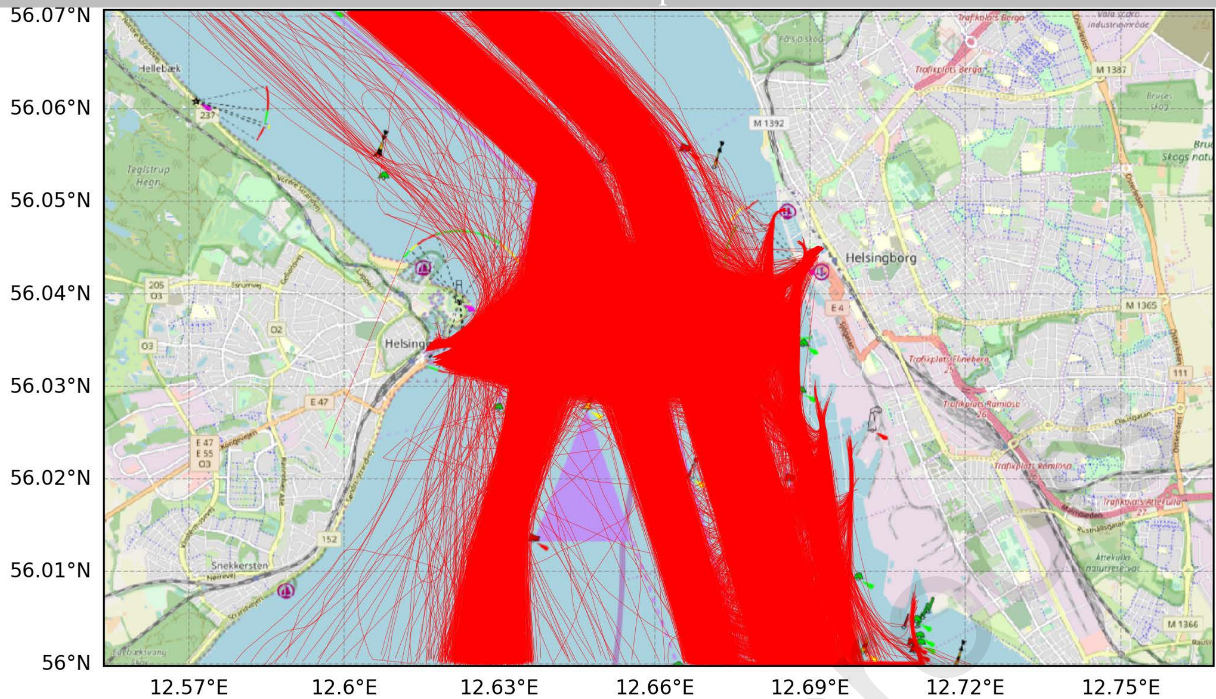

Fig. 6. Research area and ship trajectories.

4.2. Traffic patterns extraction results

According to Section 3.1.2, the start, end, and length of each trajectory are utilised as the features in the OPTICS clustering algorithm to capture the traffic patterns. As a density-based clustering algorithm, the parameter reachability distance ε has a significant and direct impact on the algorithm's performance. Compared to the DBSCAN algorithm, the most outstanding advantage of OPTICS is its ability to visualise the relationship between the ε and the clusters. The reachability distance plot is shown in Fig. 7.

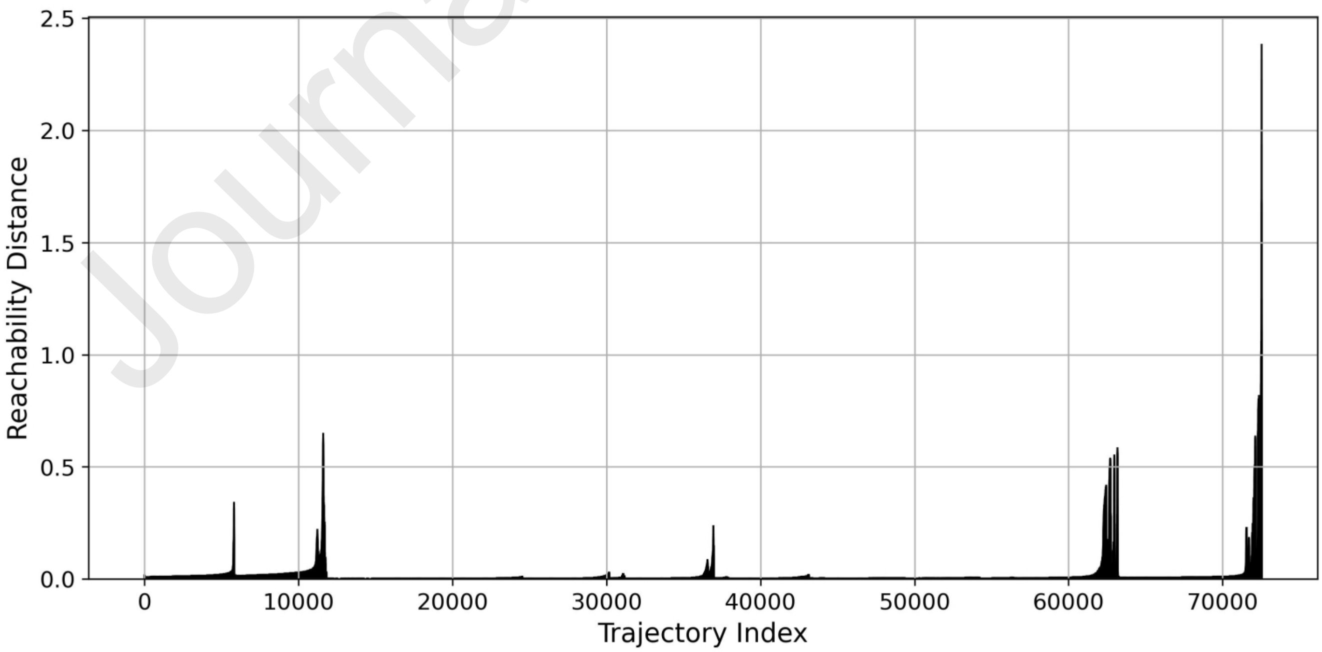

Fig. 7. Reachability distance plot.

To estimate the accuracy and effectiveness of the clustering outcome, three typical indicators are adopted: Silhouette Score (SS), Davies-Bouldin Index (DBI), and Calinski-Harabasz Index (CHI). After a series of parameter tuning experiments, the reachability distance is determined as 0.225. With a high SS (0.812), a low DBI (0.347), and a remarkably large CHI (5.58×10^5), the clustering results all fall within ideal ranges, exhibiting small intra-cluster distances and large inter-cluster distances, which confirms the effectiveness of the clustering (Xin et al., 2025b). The trajectory clusters and the corresponding number of trajectories are demonstrated in Figs. 8 and 9, respectively.

As shown in Figs. 8 and 9, Clusters 1 and 2 represent the bi-directional ferry trajectories between Helsingborg and Helsingør, jointly accounting for 69.7% of all trajectories. In addition, Clusters 3 to 5 represent the three major traffic flows sailing through the main channels, contributing a further 27.4% of the dataset. Overall, the main traffic patterns in the research area are clearly distinguishable, consisting of ferry ships crossing the traffic lanes between Helsingborg and Helsingør, as well as ships sailing along the three principal traffic lanes.

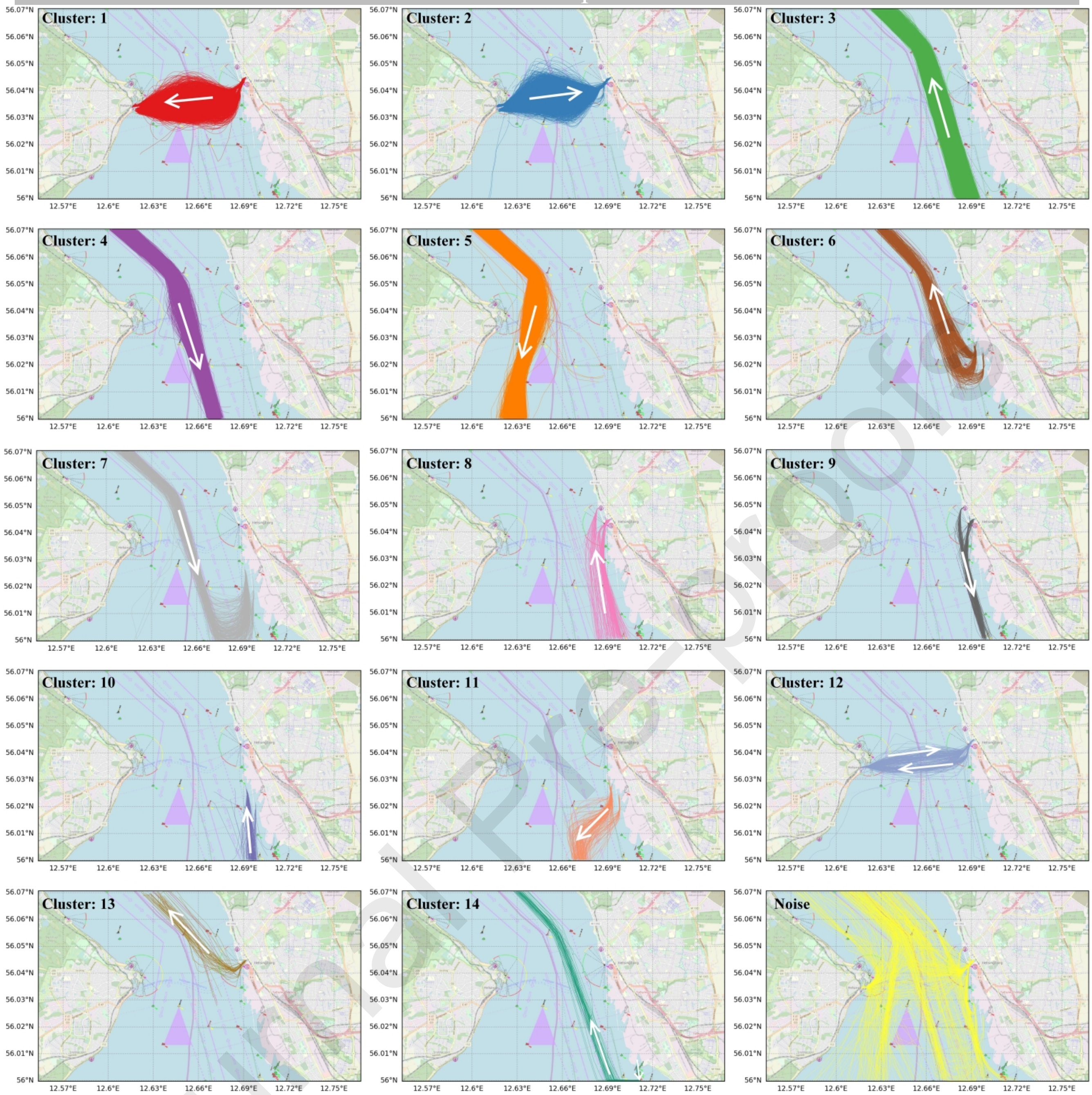

Fig. 8. Visualisation of trajectory clusters.

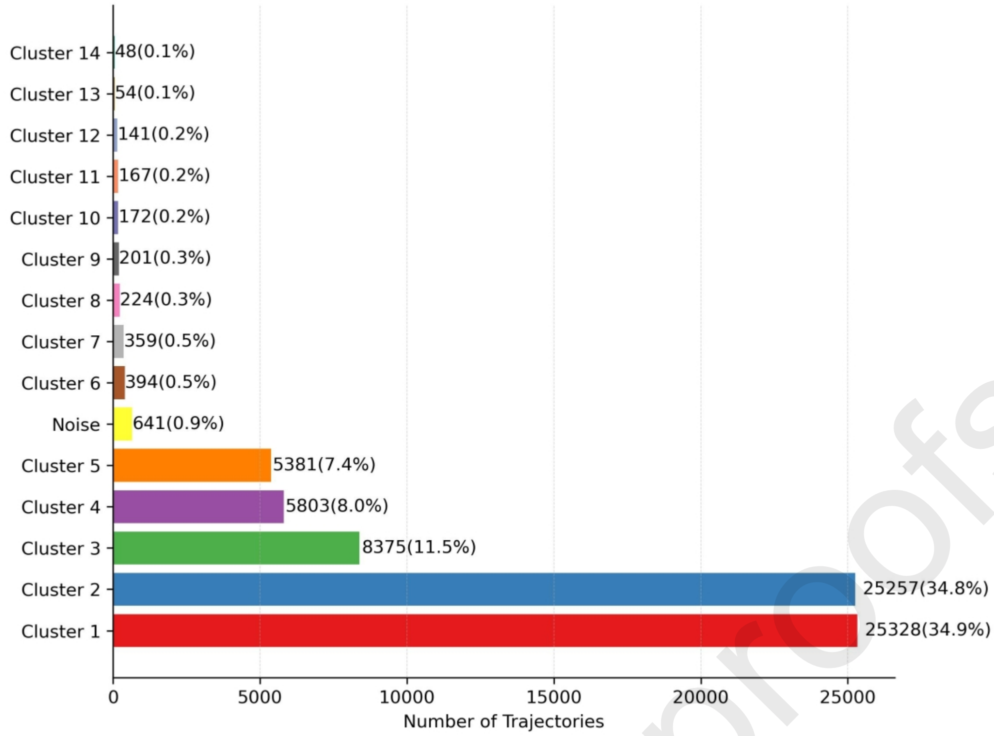

Fig. 9. Number of trajectories distribution.

The centrelines of Clusters 1 and 2 are constructed to serve as the ferry routes for behaviour identification. According to Section 3.1.2, the DTW is employed to measure the distance between trajectories, and the centrelines are constructed as shown in Fig. 10.

To determine the distance boundary between low-deviation and high-deviation trajectories, the distances between trajectories and their corresponding centreline are grouped into two clusters. According to Fig. 10, the trajectories with low deviation follow similar overall spatial trends to the constructed centrelines, indicating that the centrelines effectively capture the dominant RB patterns and can be used as representative planned routes in the subsequent behaviour identification.

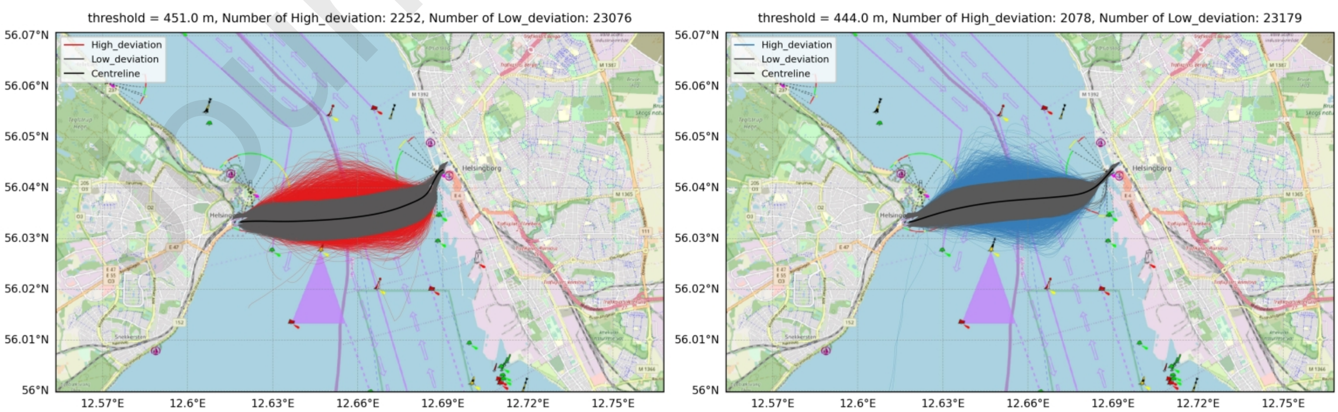

(a) Centreline of trajectories in Cluster 1 (b) Centreline of trajectories in Cluster 2

Fig. 10. Centrelines of ferry routes.

4.3. Ship behaviour identification results

To evaluate the performance of the proposed behaviour identification method, 1500 ship trajectories are randomly selected and manually labelled. The annotation is conducted in two steps. First, each trajectory is labelled as either containing a CCAB or only an RB. Second, for trajectories containing CCABs, the start and end times of the manoeuvring behaviour are manually annotated. Considering that the proposed method involves eight parameters and seven of them need to be calibrated, the labelled dataset is divided into a calibration set and an independent validation set with an 8:2 ratio. The calibration set contains 1200 trajectories, including 211 trajectories with CCABs. The validation set contains 300 trajectories, including 50 trajectories with CCABs. The similar proportion of CCAB trajectories in the two sets ensures a comparable class distribution between parameter calibration and independent validation.

Exhaustively evaluating all possible parameter combinations would be computationally expensive because the seven parameters jointly affect the behaviour identification results. Therefore, an orthogonal experimental design is adopted to reduce the parameter search space to 81 representative and mutually orthogonal parameter combinations. These 81 parameter combinations are evaluated only on the calibration set, and the parameter combination with the best overall performance is selected as the final configuration. The selected parameter combination is then directly applied to the independent validation set without further adjustment, as shown in Table 4. The evaluation is conducted at both trajectory and point levels. At the trajectory level, the metrics examine whether the method can correctly identify trajectories containing CCABs. At the point level, the metrics evaluate the consistency between the detected CCAB and the manually labelled manoeuvring behaviour, thereby assessing the accuracy of the proposed CPD-based method.

As shown in Table 4, the proposed method achieves consistent performance on the calibration and validation sets. At the trajectory level, the method obtains an accuracy of 0.9399, precision of 0.7980, recall of 0.8438, and F1-score of 0.8203 on the calibration set. On the independent validation set, the corresponding values are 0.9467, 0.8696, 0.8000, and 0.8333, respectively. The comparable results between the two sets indicate that the selected parameter configuration is not only fitted to the calibration data, but also maintains stable performance on unseen trajectories. At the point level, the method also achieves high consistency between the detected and manually labelled manoeuvring behaviours. Moreover, the performance at the point level is higher than that at the trajectory level, achieving around 0.9. This indicates that the CPD-based method can not only detect whether a trajectory contains a CCAB, but also determine the duration of CCAB. The calibrated parameters through sensitivity analysis are shown in Table 5.

Table 4. Performance of the proposed behaviour identification method.

Performance metrics	Trajectory level		Point level	
	Calibration set	Validation set	Calibration set	Validation set
Accuracy	0.9399	0.9467	0.8861	0.8893
Precision	0.7980	0.8696	0.9125	0.8935
Recall	0.8438	0.8000	0.9289	0.9547
F1	0.8203	0.8333	0.9206	0.9231

Table 5. Values of adopted threshold parameters

Parameter	Value	Parameter	Value
$\tau_{dist}^{\text{Peak}}$	1.000	$\tau_{\Delta COG}^{\text{Peak}}$	10°/180°
τ_{dist}^{Amp}	0.600	$\tau_{\Delta COG}^{\text{Amp}}$	0.200
$\tau_{dist}^{\text{Prop}}$	0.400	$\tau_{\Delta COG}^{\text{Prop}}$	0.300
τ_{ROT}	15°/min	$\tau_{Decline}$	0.150

As shown in Fig. 10, the boundary between the high-deviation and low-deviation trajectories is determined, which can be adopted as the empirical upper bound of normal lateral deviation. As shown in Eq. (3), the normalised peak distance exceeding 1 is treated as indicative of noticeable departure from the planned route. Accordingly, the $\tau_{dist}^{\text{Peak}}$ is set to 1. Similarly, the value of $\tau_{\Delta COG}^{\text{Peak}}$ is set to 0.056, corresponding to a normalised relative course change of $10°$. τ_{dist}^{Amp} represents the minimal ratio between the rising or falling amplitude of the distance and its peak value. A value of 0.6 is adopted to prevent misclassifying trajectories that show a prominent peak but only a minor change in amplitude (Fig. 4). In contrast to the distance variation, the ΔCOG typically exhibits a three-phase pattern (e.g., rise–fall–rise or fall–rise–fall), corresponding to the departure from the planned route, return towards it, and subsequent return to the planned course. As the ΔCOG variation typically exhibits a more pronounced change in return phase, the $\tau_{\Delta COG}^{\text{Amp}}$ is determined as 0.2, which is lower than τ_{dist}^{Amp}. For ship collision avoidance behaviours, Rule 8(b) of COLREGs states that *"a succession of small alterations of course should be avoided"*. To satisfy this requirement, the CAB during both the departure and the return phases should be sufficiently noticeable by other ships. Accordingly, the thresholds $\tau_{dist}^{\text{Prop}}$ and $\tau_{\Delta COG}^{\text{Prop}}$, which denote the minimal proportion of rising or falling phase, are set to 0.2. This prevents trajectories involving a succession of minor course alterations from being misidentified as CCABs, which would otherwise appear as a large proportion of rising or falling phases. The τ_{ROT} is determined as 10°/min, indicating that the average ROT of manoeuvring should exceed 10°/min. The change point penalty $\tau_{Decline}$ is fixed at 0.1, which represents the minimal decline percentage of cost when adding a change point.

To evaluate the contribution of each kinematic feature to the performance of behaviour identification, the Analysis of Variance (ANOVA) is employed to analyse the main effect based on the results of an orthogonal experimental design. The relative importance of each threshold factor in different performance metrics is illustrated in Fig. 11. Overall, $\tau_{\Delta COG}^{\text{Peak}}$ is the most influential kinematic feature (23%~35.9%), suggesting that the magnitude of course deviation from the planned route is the primary characteristic of

CCABs. This aligns with COLREGs, which require course alterations to be *"large enough to be readily apparent to another vessel observing visually or by radar"*. $\tau_{Decline}$ exhibits the second highest importance (21.8%~28.7%), as it controls the strictness with which decreasing trends in the cost function are interpreted as behavioural changes. τ_{ROT}, $\tau_{\Delta COG}^{\text{Amp}}$, $\tau_{\Delta COG}^{\text{Prop}}$, and $\tau_{dist}^{\text{Prop}}$ show moderate contributions (up to 15.8%), suggesting that these features capture the proportional and temporal characteristics of manoeuvring, but play a secondary role relative to peak course deviation. Finally, τ_{dist}^{Amp} shows the lowest importance (less than 2.6%), which indicates that normal RBs rarely exhibit significant short-term variations in kinematic features (Fig. 4).

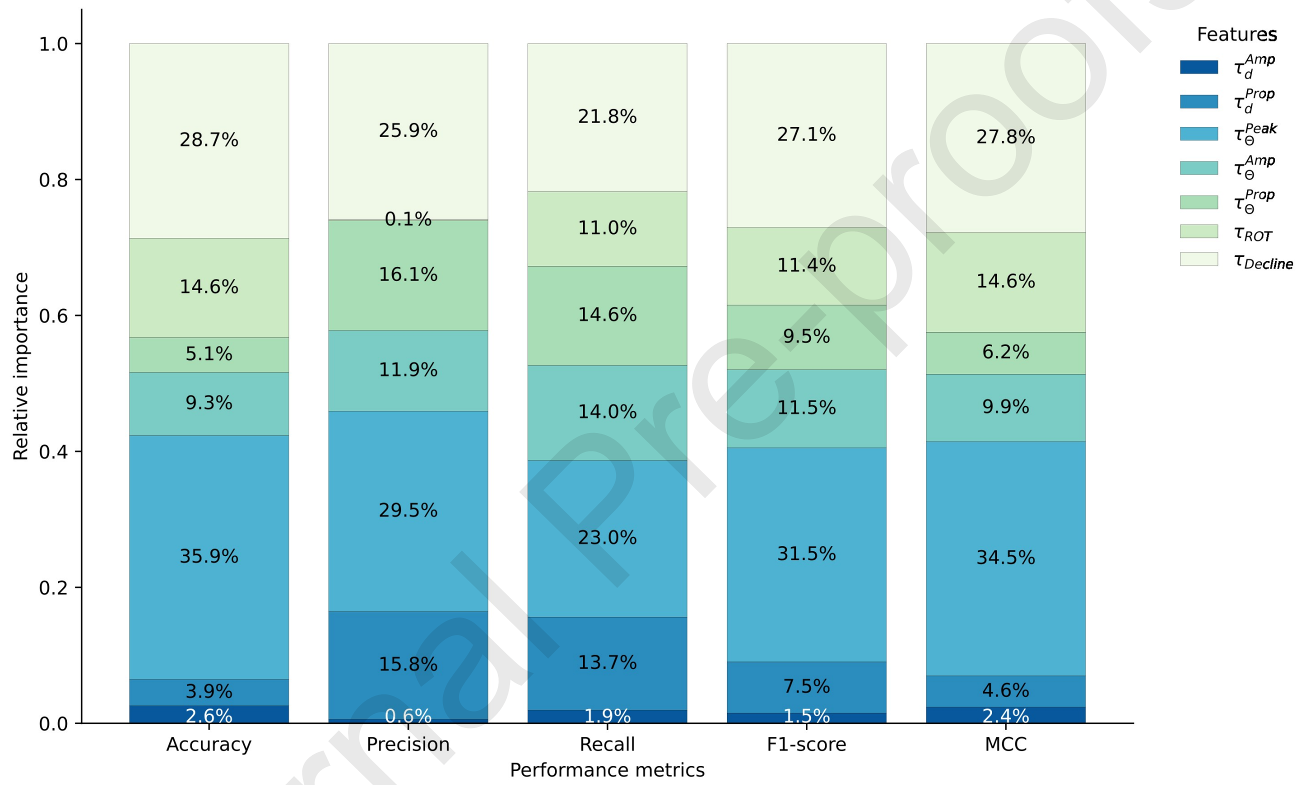

Fig. 11. Relative importance of each threshold factor.

To evaluate the effectiveness and interpretation of the proposed ship behaviour identification method and to verify the rationality of the thresholds determined by the orthogonal experimental design, a representative trajectory containing two change points is analysed in detail (Fig. 12). Following Algorithm 1, the total cost of the number of change points K varying from 0 to K_{max} is evaluated, enabling a demonstration of how the cost function is used to identify the ship behaviours.

Zero change point (*K*=0): When no change point is introduced, the entire trajectory is identified as a single behaviour. Although both the distance and ΔCOG show manoeuvring characteristics, the high proportion of fluctuation leads to a large RB penalty in the cost function. As a result, the trajectory is determined as an RB, yielding a total cost of 65.5 (Fig. 12(a)). This provides a baseline for subsequent comparisons.

One change point (*K*=1): Introducing one change point allows the algorithm to identify one CCAB. However, as shown in Fig. 12(b), the rising proportion in the distance and ΔCOG are severely affected by long-term fluctuations, causing the indices $dist_{\mathrm{Prop}}^{\mathrm{Rise}}$ and $\Delta COG_{\mathrm{Prop}}^{\mathrm{Rise}_1}$ to remain below their corresponding thresholds. Meanwhile, the low distance values in fluctuation indicate that the ship remains close to the planned route, leading to a high RB penalty. Consequently, the total cost only slightly decreases to 58 (−11.5% relative to *K*=0).

Two change points (*K*=2): When two change points are included, the cost function successfully extracts a CCAB that satisfies most threshold criteria, leading to a low total cost. The distance exhibits a clear rising-falling structure with sufficient proportion and amplitude, matching the characteristics of a representative manoeuvre. In contrast, although the ΔCOG exhibits a trend of rising-falling-rising, which is consistent with the evolution pattern of CABs, the trajectory demonstrates a tendency to approach the planned route before the first change point, causing the first rising phase amplitude $\Delta COG_{\mathrm{Amp}}^{\mathrm{Rise}_1}$ to fall below its corresponding threshold. According to Fig. 12(c), since the RBs exhibit fluctuations and are not consistent with the trends in distance and ΔCOG observed in typical CABs, these two segments are accurately identified as RBs. Owing to the accurate identification of two RBs, the total cost drops sharply to 21.8, representing reductions of 62.5% and 67.2% compared to the cost with *K*=1 and *K*=0, well beyond the threshold $\tau_{Decline}$. This identification process highlights that the identification algorithm, considering kinematic feature evolution throughout the entire collision avoidance process, can accurately determine the ship behaviours.

Three change points (*K*=3): According to Fig. 12(d), further increasing the number of change points does not change the results of behaviour identification, and the outcome remains identical to that of *K*=2. With $K = 2$, the model achieves precise behaviour identification, and all identified manoeuvring and RBs are physically interpretable. When the number of change points increases to $K = 3$, the algorithm merely subdivides an existing RB into two adjacent sailing parts without introducing any change in manoeuvring pattern. As a result, the total cost remains constant and fails to achieve the 10% decline requirement of $\tau_{Decline}$. This behaviour persists when K increases to three or more, confirming that *K*=2 is the optimal and stable solution.

Overall, the analysis demonstrates that the established cost function effectively considers kinematic feature evolution throughout the entire collision avoidance process and thus can accurately identify the ship behaviours, while maintaining high interpretability. The rationality and general applicability of thresholds are confirmed through orthogonal experimental design based on the labelled dataset.

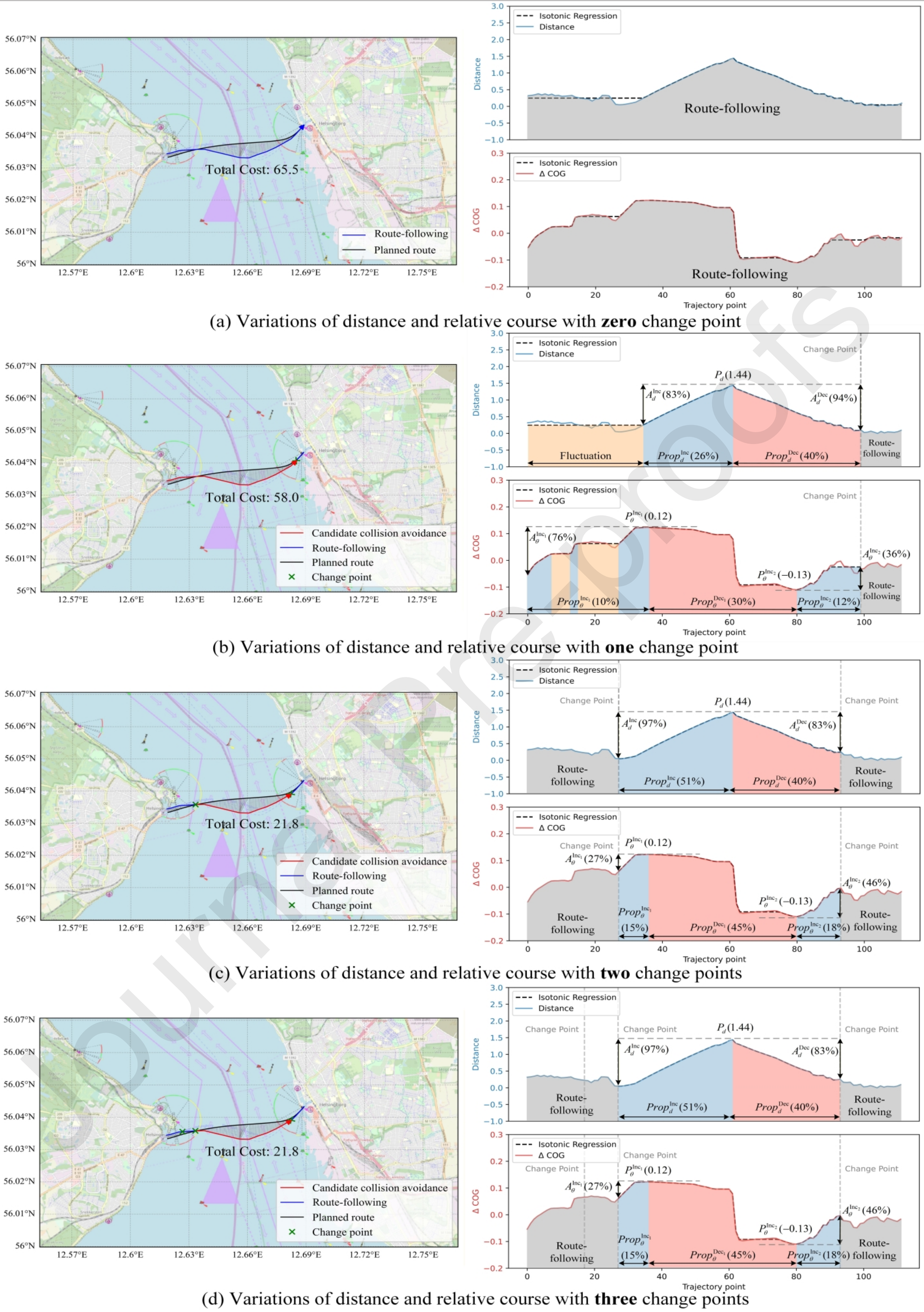

Fig. 12. Illustration of CPD in a typical trajectory.

4.4. Ship encounter extraction results

Unlike the conventional classification based solely on geometrical relations, the proposed critical encounter scenarios extraction method incorporates the extracted CCABs to derive an intention-informed encounter taxonomy (Algorithm 2). For example, $Cross_{\mathrm{bow2stern}}$ indicates that the ship is intentionally taking manoeuvring action so that the passing situation changed from *"bow passing"* to *"stern passing"* relative to the target ship. To illustrate the mechanism of the proposed algorithm and evaluate its performance in a real-world case, a multi-ship encounter scenario, which contains a $Cross_{bow}$ and $Cross_{bow2stern}$ encounter types, is selected to apply the algorithm.

Fig. 13 illustrates the reference trajectory, which follows along the planned route without any evasive action. Along this reference trajectory, the own ship would sequentially pass ahead of ship A and ship B at short distances of 0.59 and 0.164 nm. These passing conditions indicate that, without a manoeuvre, the own ship would experience two consecutive $Cross_{bow}$ encounter situations, which represent a hazardous multi-ship encounter. In terms of the real manoeuvring trajectory, by altering its course to starboard, the own ship passes ahead of ship A at a distance of 1.081 nm (Fig. 14). This distance is 1.83 times larger than the 0.59 nm caused by the reference trajectory, indicating that the manoeuvre is intended to pass ship A at a safer distance. For ship B, the passing condition changes from $Cross_{bow}$ to $Cross_{stern}$, which shows that the own ship follows the requirement of COLREGs by passing astern of the target ships to ensure navigational safety (Fig. 14). Given that both ship A and B are passed at significantly safer conditions by taking manoeuvring action, this encounter is determined as a multi-ship encounter scenario. These results demonstrate the effectiveness of the proposed intention-informed encounter extraction approach. By comparing the reference and real trajectories, the method can identify the target ships, which the own ship intends to avoid.

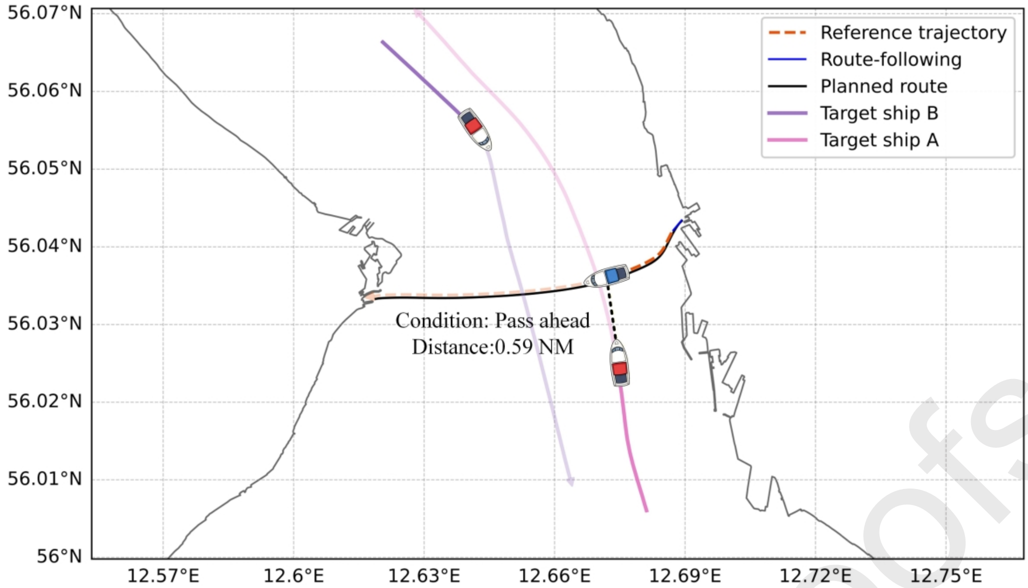

(a) Passing condition of target ship A

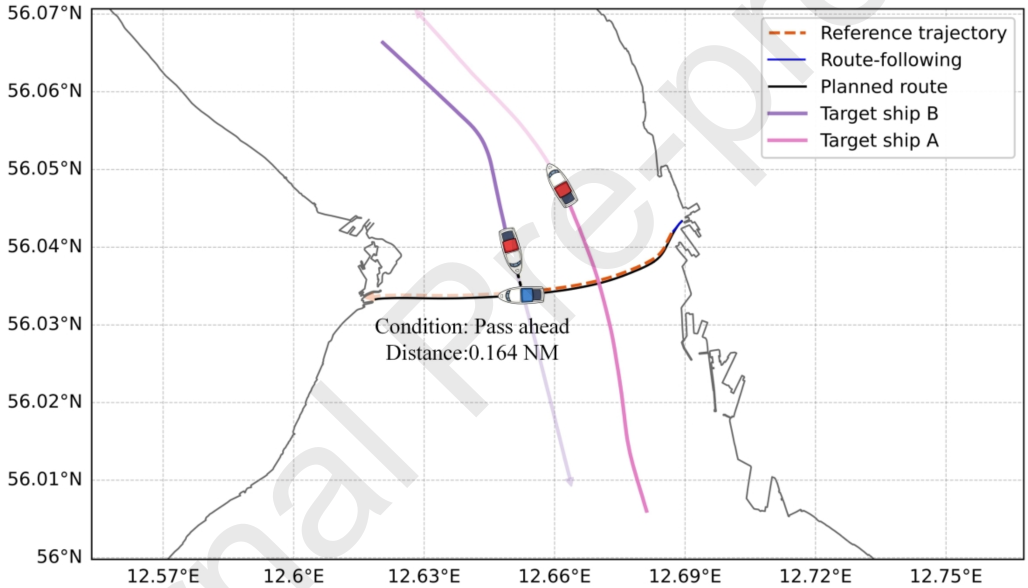

(b) Passing condition of target ship B

Fig. 13. Pass condition of the reference trajectory.

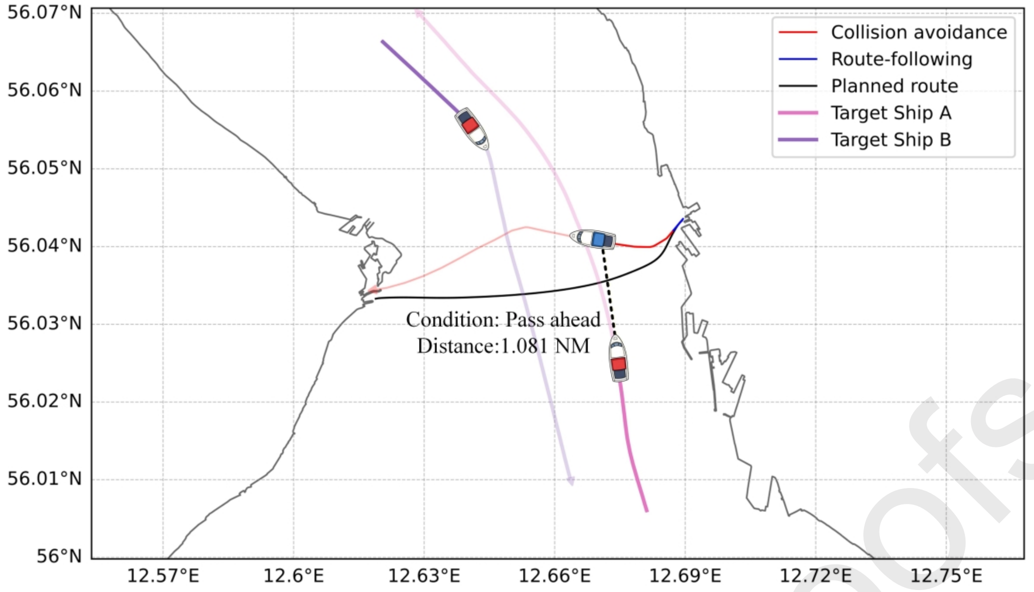

(a) Passing condition of target ship A

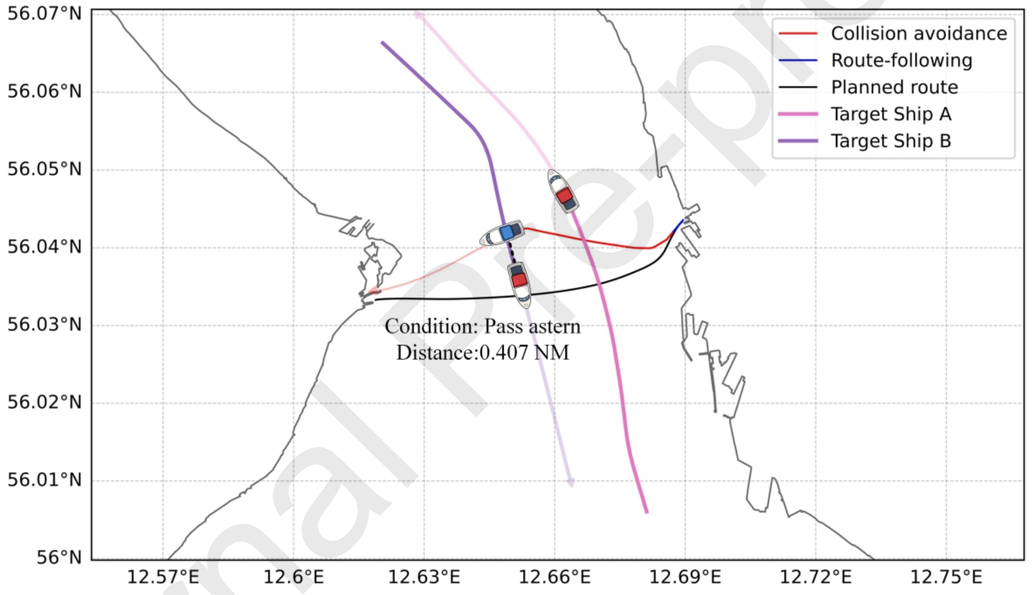

(b) Passing condition of target ship B

Fig. 14. Pass condition of the real manoeuvring trajectory.

Figs. 13 and 14 illustrate the mechanism of the proposed critical encounter extraction method; however, the performance of this method in real-world encounter extraction is still unknown. Therefore, based on the labelled parameter calibration and independent validation dataset in behaviour identification, the critical encounters in these two sets are labelled to examine the performance of the proposed critical encounter extraction method. Specifically, 319 and 60 critical encounters are recognised and labelled in parameter calibration and independent validation data sets, respectively. To compare the effectiveness of encounter extraction with relative and recent methods, the comparison methods A (Xin et al., 2025b) and B (Yu et al., 2025) are adopted. The core of comparison method A is employing thresholds to filter critical encounters, and based on method A, the core of comparison method B is to establish the Evolving Graph Sequences (EGS) to represent the evolution of critical encounters and evaluate the structural similarities between snapshots within the EGS to extract critical encounters. The performance metrics in critical encounter scenario extraction among the proposed method and two comparison methods are shown in Table 6.

Table 6. Performance comparison of encounter extraction methods.

Performance metrics		Calibration set	Validation set
Proposed method	Accuracy	0.9714	0.9677
	Precision	0.8359	0.8478
	Recall	0.6708	0.6500
	F1	0.7443	0.7358
Comparison method A	Accuracy	0.5710	0.5267
	Precision	0.0843	0.0681
	Recall	0.8934	0.9000
	F1	0.1541	0.1266
Comparison method B	Accuracy	0.5427	0.5006
	Precision	0.0832	0.0678
	Recall	0.9436	0.9500
	F1	0.1529	0.1267

According to Table 6, the proposed method shows comparable performance on the calibration and validation sets. The accuracy, precision, recall, and F1-score on the validation set are close to those obtained on the calibration set, indicating that the selected parameters maintain stable performance on unseen data.

With respect to precision and recall, the proposed method achieves consistently high precision on both the calibration and validation sets, with values of 0.8359 and 0.8478, respectively. Since precision is defined as $\frac{TP}{(TP+FP)}$, this indicates that most extracted critical encounters are true positives and the number of false positives is relatively small. In contrast, the recall values are lower, at 0.6708 and 0.6500 on the calibration and validation sets, respectively. Since recall is defined as $\frac{TP}{(TP+FN)}$, this indicates that some critical encounters are missed. Therefore, the proposed method can be regarded as relatively conservative: it reduces the risk of incorrectly extracting non-critical ship pairs as critical encounters, but this is achieved at the cost of increasing false negatives. Nevertheless, the F1-scores of 0.7443 and 0.7358 indicate that the proposed method maintains a better balance between precision and recall than the comparison methods.

The two comparison methods show a contrasting performance pattern. Although they achieve high recall on both datasets, their precision remains very low. For example, on the calibration set, comparison methods A and B achieve recall values of 0.8934 and 0.9436, but their precision values are only 0.0843 and 0.0832, respectively. This indicates that these methods can identify most critical encounters, but they also incorrectly classify a large number of non-critical ship pairs as critical encounters, leading to many false positives. Consequently, their F1-scores are much lower than that of the proposed method.

This difference can be attributed to the information used in encounter extraction. According to COLREGs, the encounters are linked with evasive action. As shown in Table 7, involving evasive actions is the necessary condition for forming an encounter. However, the comparison methods mainly rely on ship-to-ship relative motion indicators, such as DCPA, TCPA, and relative distance. These indicators are effective for quantifying collision risk, but they are challenging to examine whether a manoeuvre is actually present or whether this manoeuvre is associated with a specific avoided target ship. By contrast, the proposed method first identifies CCABs and then links this behaviour to the corresponding avoided target ship by comparing the observed trajectory with a reference route-following trajectory. Overall, the comparison results demonstrate that the proposed method provides more reliable and balanced critical encounter extraction.

Table 7. Definition of encounter types in COLREGs.

Encounter type	Definition
Overtaking	Any vessel overtaking any other shall **keep out of the way** of the vessel being overtaken.
Head-on	Each shall **alter her course to starboard** so that each shall pass on the port side of the other.
Crossing	The vessel which has the other on her own starboard side shall **keep out of the way** and shall, if the circumstances of the case admit, avoid crossing ahead of the other vessel.

Based on the critical encounter extraction method, the distributions of critical encounters are illustrated in Fig. 15. The total number of extracted critical encounters is 2602 in Cluster 1 and 2238 in Cluster 2, indicating that ferries operating in the two directions experience a comparable number of critical encounters. The two clusters also show similar distributions in terms of the number of target ships. Encounters with one target ship, the two-ship encounters, account for the largest proportion, with more than 60%. As the number of target ships increases, the proportion of encounter scenarios decreases rapidly. This indicates that most extracted critical encounters are two-ship encounters, while multi-ship encounters are less frequent but still present in both traffic directions.

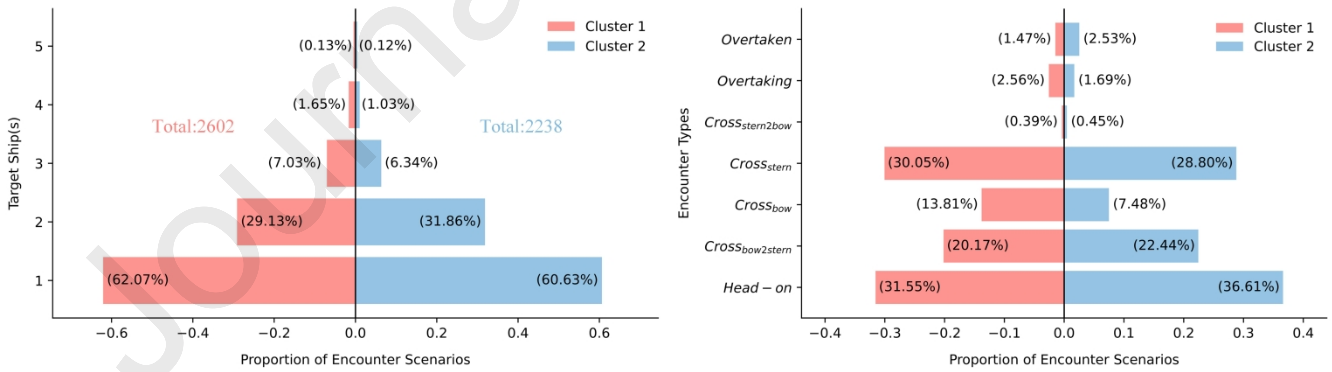

(a) Distribution of encounter scenarios by number of target ships (b) Distribution of encounter types

Fig. 15. Distribution of two-ship and multi-ship encounter scenarios.

Fig. 15(b) further shows the distribution of encounter types. Head-on and crossing encounters dominate in both clusters, while overtaking and overtaken encounters account for only a small proportion. This suggests that, in the ferry corridor, critical encounters are mainly associated with opposite-direction traffic and crossing traffic.

For crossing encounters, the results show a clear tendency towards stern passing. In this study, $Cros$

s_{stern} and $Cross_{bow2stern}$ represent cases in which the own ship takes evasive action to pass astern of the target ship. Together, these two types account for 78.0% of all crossing encounters in Cluster 1 and 86.6% in Cluster 2. In particular, the relatively high proportion of $Cross_{bow2stern}$ cases indicates that many potentially risky bow-crossing situations are converted into stern-passing situations through CAB. This tendency is consistent with the intention of COLREGs Rule 15, which requires the give-way vessel to avoid crossing ahead of the other vessel.

In contrast, $Cross_{stern2bow}$ accounts for only 0.39% in Cluster 1 and 0.45% in Cluster 2. Compared with the high proportions of $Cross_{stern}$, this indicates that when the reference trajectory already allows the own ship to pass astern of the target ship, ships rarely take manoeuvres that change the passing condition to bow crossing. Instead, most ships tend to maintain stern passing and increase the passing distance.

4.5. Collision avoidance behaviour analysis

In ship encounters, the COLREGs distinguish the obligations of the involved ships by assigning different responsibilities, which are commonly categorised as the give-way and stand-on roles. Motivated by this role differentiation, this section conducts a comparative analysis of collision-avoidance actions from both ships' perspectives, with the objective of characterising the differences in manoeuvre timing, action magnitude, and response patterns as observed in practice. Accordingly, Figs. 16-18 compare the CABs of give-way and stand-on ships in different crossing encounter types from three perspectives: the timing of triggering avoidance action, the minimum distance between ships, and the magnitude of avoidance action. The analysis focuses on the $Cross_{bow}$, $Cross_{stern}$, and $Cross_{bow2stern}$ encounter types.

Fig. 16 shows the distribution of relative distance when taking evasive action, which serves as the timing of triggering CAB. Overall, give-way ships exhibit larger initiation distances, whereas stand-on ships tend to initiate evasive action at shorter distances, which is consistent with their role-dependent obligations under COLREGs: stand-on vessels typically maintain course and speed and resort to manoeuvring primarily when collision cannot be avoided by the give-way vessel alone. Meanwhile, the distributions of give-way ships are more dispersed. The variance for stand-on ships is about 0.1-0.17, clearly lower than the 0.21-0.35 observed for give-way ships. This suggests that compared to the stand-on ships, the give-way ships show greater strategy variability in when to trigger evasive action.

The stern-passing crossing cases ($Cross_{stern}$, and $Cross_{bow2stern}$) provide a clear setting in which give-way and stand-on responsibilities can be distinguished. For these two situations, give-way ships exhibit similar mean and median relative distance between 1.65NM and 1.69NM, respectively, which exceed the corresponding values of about 1.22NM and 1.25NM for stand-on ships. This suggests that, in stern-passing situations, evasive action by give-way ships is typically initiated roughly 0.4NM earlier (in terms of relative distance) than that by stand-on ships. By contrast, in $Cross_{bow}$ situation, the distribution of relative distance in two responsibilities is similar (give-way ≈ 1.59NM and stand-on ≈ 1.48/1.47NM), indicating that the bow-passing scenario does not exhibit the typical pattern of earlier action by give-way ships.

In $Cross_{stern}$, and $Cross_{bow2stern}$, the numbers of give-way cases (1662 and 1146) are 3.73 and 3.03 times those of stand-on cases, whereas in $Cross_{bow}$ the number of give-way cases is only 243, accounting for less than half of the stand-on cases. Overall, the observed give-way ships more frequently adopt stern-passing strategies in crossing encounters, which is consistent with the COLREGs suggesting avoiding passing ahead of other ships, when circumstances permit.

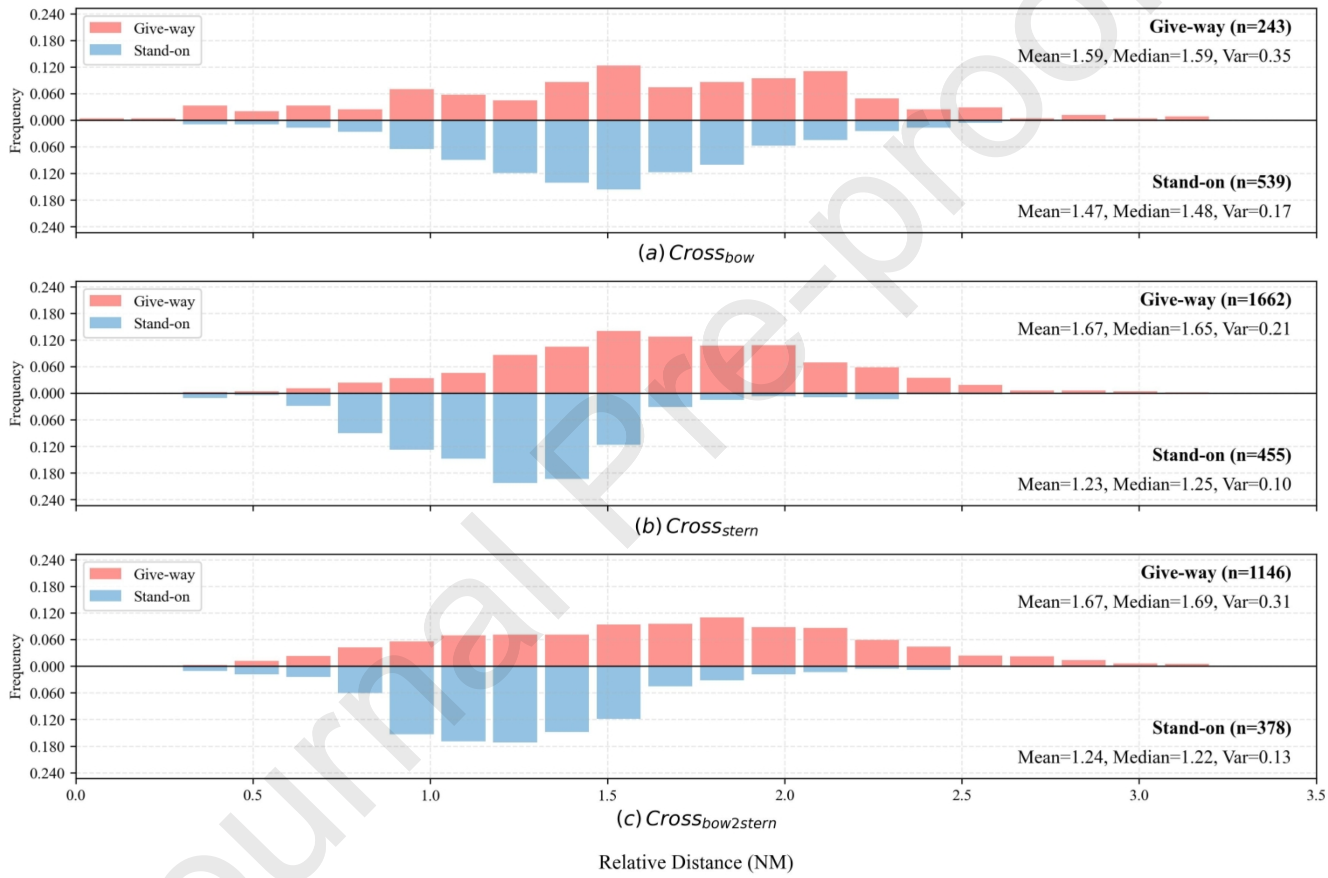

Fig. 16. Distribution of relative distance when taking evasive action.

Fig. 17 presents the distribution of the minimum distance between ships during collision avoidance manoeuvring, which characterises the safety distance maintained throughout the collision avoidance behaviour. As shown in Fig. 17, the distributions of the minimum distance for give-way and stand-on ships are similar in both $Cross_{stern}$ and $Cross_{bow2stern}$ situations. For each encounter situation, give-way and stand-on ships exhibit comparable variances, and similar means and medians, which indicates that once a stern-passing strategy is adopted, give-way and stand-on ships tend to maintain a similar level of safety distance. Even though, both $Cross_{stern}$ and $Cross_{bow2stern}$ situations involves stern passing, $Cross_{stern}$ exhibits noticeably larger mean and median minimum distances than $Cross_{bow2stern}$ (Fig.

17). This difference is likely because $Cross_{bow2stern}$ represents a transition from an initially bow-passing situation to a stern-passing outcome. Under comparable avoidance action magnitude, such a transition typically results in smaller minimum distances than in $Cross_{stern}$ situation, where stern passing is established more directly.

In contrast, $Cross_{bow}$ exhibits a markedly different pattern. For give-way ships, the mean and median minimum distances are 0.3 and 0.28NM, substantially smaller than those for stand-on ships (mean: 0.50NM and median: 0.45NM). This contrasts with the stern-passing encounters, where give-way and stand-on ships maintain comparable safety distance. The reduced minimum distances in $Cross_{bow}$ suggest that give-way ships operate under more constrained conditions in bow-passing situations.

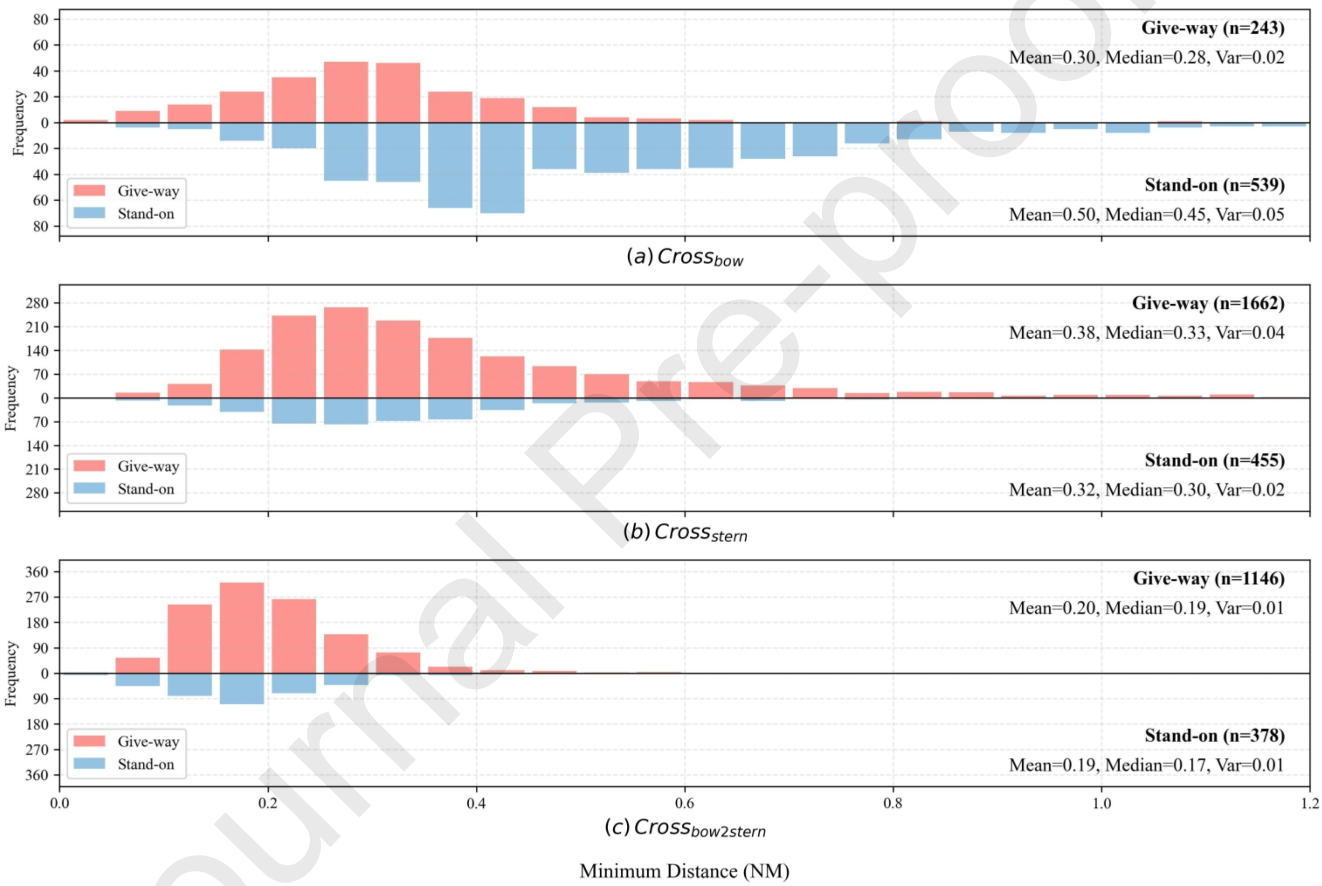

Fig. 17. Distribution of minimum distance between ships.

As shown in Fig. 18, substantial course changes are observed in both the deviation and recovery stages. During the deviation stage, the mean course changes range from approximately 23.86° to 39.05°, indicating that ships usually take clear manoeuvring actions to avoid collision. Among the three encounter types, $Cross_{bow2stern}$ exhibits the largest deviation magnitudes, with the mean and median values generally exceeding 33°. This is reasonable because $Cross_{bow2stern}$ represents a transition from a potential bow-passing situation to a stern-passing situation, which usually requires more pronounced course alterations to change the passing relation and reduce collision risk.

The recovery stage also shows notable course changes, although the magnitudes are generally smaller than those in the deviation stage, especially for $Cross_{stern}$ and $Cross_{bow2stern}$. The absolute mean and median values during recovery remain approximately within the range of 21°–31°, indicating that ships do not immediately return to planned route after the main avoidance deviation. Instead, they continue to adjust their course to recover towards the planned route after the conflict has been resolved. This confirms that collision avoidance behaviour should be regarded as a complete deviation–recovery process rather than a single course alteration. For the same encounter type, the differences in maximum course changes between give-way and stand-on ships are relatively small compared with the differences observed in relative distance. This suggests that, in the extracted critical encounters, both give-way and stand-on ships may perform comparable manoeuvring adjustments once collision risk occurs.

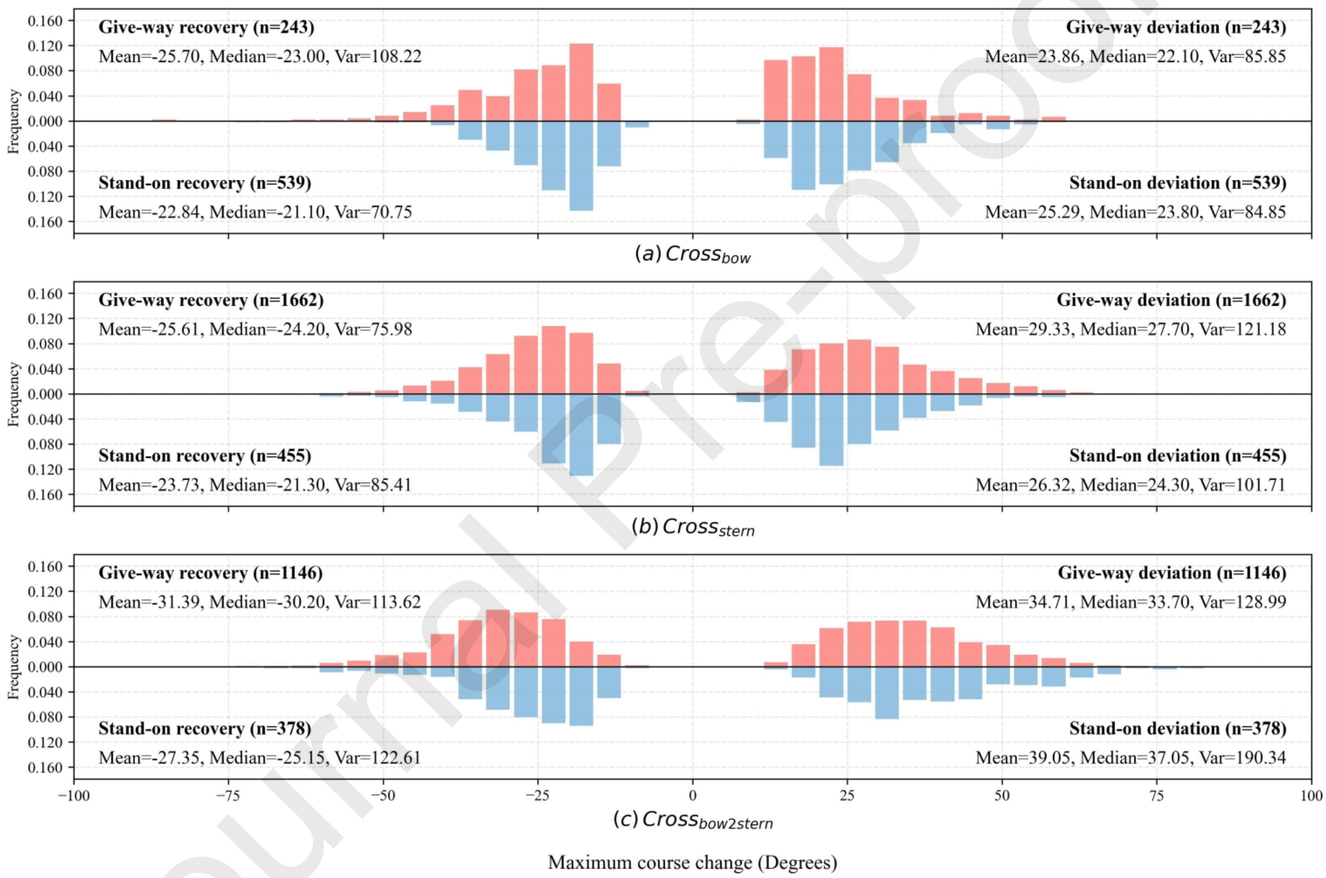

Fig. 18. Distribution of maximum course change in deviation and recovery stages.

To investigate the relationships among avoidance timing, safety distance, and avoidance magnitude across different crossing encounter types in this study area, a comparative analysis of Figs. 16-18 is conducted.

For the two stern-passing situations ($Cross_{stern}$ and $Cross_{bow2stern}$), give-way and stand-on ships exhibit broadly consistent behavioural patterns. Give-way ships tend to initiate collision avoidance actions at larger relative distances than stand-on ships, whereas the two roles maintain comparable minimum distances and avoidance magnitudes. Notably, although stand-on ships manoeuvre at shorter distances, they still achieve similar safety margins and manoeuvre amplitudes, suggesting that the primary difference between these stern-passing cases lies in the timing of avoidance initiation rather than the intensity of manoeuvring.

In contrast, $Cross_{bow}$ exhibits a distinctly different behavioural pattern. Although COLREGs advise avoiding crossing ahead where circumstances permit, and bow-passing is generally associated with higher collision risk, some give-way ships are nevertheless observed to pass ahead of the other ship. In this situation, the initiation for evasive action timing of give-way ships becomes similar to that of stand-on ships, which is different from the earlier initiation observed in $Cross_{stern}$ and $Cross_{bow2stern}$ situations. In addition, although give-way ships in $Cross_{bow}$ exhibit avoidance magnitudes similar to those of stand-on ships, the resulting minimum distances are significantly smaller than those of stand-on ships. Overall, the joint pattern of avoidance timing, safety distance, and manoeuvre magnitude suggests that these $Cross_{bow}$ situations are likely associated with constrained conditions in which early avoidance is not feasible. Consequently, give-way ships may adopt a bow-passing outcome and, despite substantial actions, are unable to maintain larger safety distances.

5. Discussion and implications

This study proposes a ship behaviour identification method based on a CPD method and an intention-informed encounter extraction method for obtaining critical encounter scenarios that reflect real CABs. By jointly evaluating the multiple kinematic features, the proposed method enhances robustness and interpretability. Then, the intention-informed extraction further reduces the impact of false manoeuvre detections by comparing the real trajectory with the reference trajectory, ensuring that the extracted encounters contain meaningful ship–to–ship interactions rather than standard route-following behaviours. The case study also demonstrates that the method can successfully extract different types of avoidance intentions.

5.1. Applicability across different navigational environments

The applicability of the proposed method is closely related to the characteristics of the navigational environment. The ferry corridor in Section 4 provides a suitable initial test bed because ships usually follow clear intended routes and collision avoidance manoeuvres are often substantial due to the short voyage distance and the nearly perpendicular crossing of the main traffic flow. Under such conditions, the deviation-recovery-stabilisation pattern relative to the planned route can be clearly characterised. However, this also means that the validation in the ferry corridor alone is insufficient to demonstrate that the method performs well in more diverse navigational environments.

To further examine the applicability of the method in various navigational environments, an additional analysis is conducted in an extended water area that includes the ferry corridor, bridge area, dredged route, and TSSs, as shown in Fig. 19. A total of 1000 trajectories are manually labelled and used for sensitivity analysis and parameter calibration. The calibrated parameter set with the best overall performance is then compared with that obtained from the ferry corridor, as shown in Tables 8 and 9. The results show that the proposed behaviour identification method maintains acceptable performance in the extended water area, with an accuracy of 0.8300, precision of 0.8206, recall of 0.7190, and F1-score of 0.7665. Although these values are lower than those obtained in the ferry corridor, the precision remains almost unchanged. Given that $Precision = \frac{TP}{TP+FP}$, the almost unchanged precision indicates that most detected manoeuvring behaviours are still correctly identified. The decrease in recall is reasonable because the extended water area contains more heterogeneous navigational conditions and more diverse manoeuvring behaviours. Compared with the ferry corridor, where avoidance actions are usually more substantial, ships in the extended area may conduct smaller course alterations at longer distances (Figs. 19 (b) and (c)). Such behaviours produce less noticeable deviation-recovery patterns relative to the planned route and are therefore more difficult to distinguish from normal route-following behaviour using a unified parameter set, leading to higher FN. This explains why the method can still provide reliable detections when a manoeuvre is identified, while some less substantial manoeuvres may be missed.

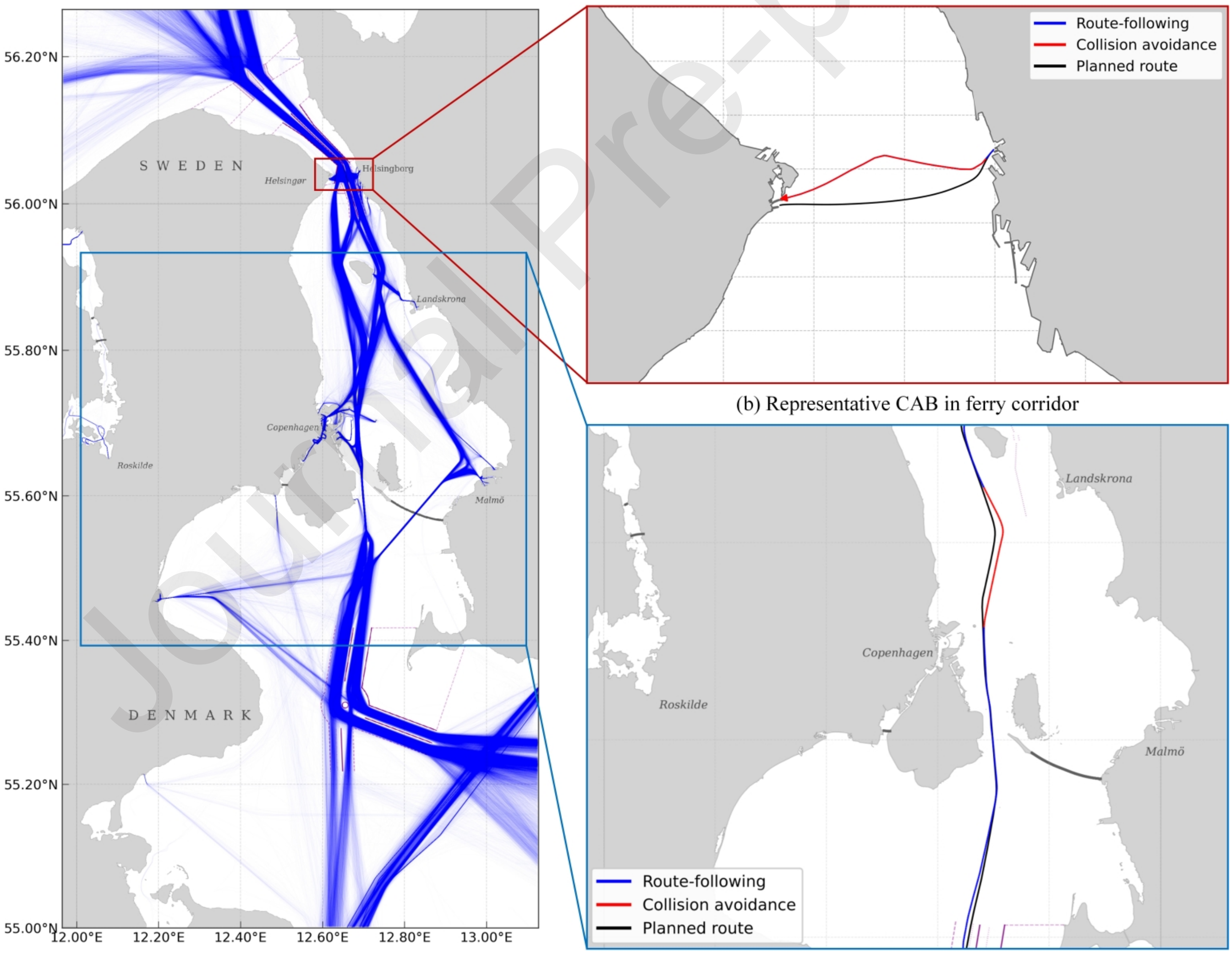

(a) Extended water area
(b) Representative CAB in ferry corridor
(c) Representative CAB in extended structured waterway

Fig. 19. The extended water area and representative CABs.

The calibrated parameters further support this interpretation. Most thresholds decrease in the extended water area compared with the ferry corridor (Table 9), suggesting that collision avoidance manoeuvres in more general structured waterways tend to involve smaller deviations from the planned route and less substantial course changes. This is consistent with the fact that ships in less constrained or longer-distance encounters may take earlier and milder evasive actions, rather than making large course alterations as observed in the ferry corridor. The only exception is τ_{ROT}, which remains at 15°/min. It suggests that, even when the total course deviation and route deviation are smaller, a detectable collision avoidance manoeuvre still needs to exhibit a sufficiently clear short-term turning process. In other words, ships in the extended water area may perform smaller evasive actions, but these actions can still involve a distinct local turning pattern that distinguishes them from normal course fluctuations. In addition, $\tau_{Decline}$ is not applied in the extended water area. This parameter represents the required reduction in the total trajectory cost when introducing additional change points. In short ferry voyages, identifying a manoeuvring behaviour can substantially reduce the total cost because the manoeuvre occupies a relatively large proportion of the trajectory. In longer voyages, however, a local manoeuvring behaviour may contribute only a small proportion of the total trajectory cost. As a result, using $\tau_{Decline}$ may suppress the detection of true manoeuvring behaviours in longer trajectories.

Table 8. Performance of the behaviour identification method in the ferry corridor and extended waterway.

Water area	Accuracy	Precision	Recall	F1-score
Ferry	0.9399	0.7980	0.8438	0.8203
Extended	0.8300	0.8206	0.7190	0.7665

Table 9. Values of adopted threshold parameters in the ferry corridor and extended waterway.

Parameter	Value (Ferry)	Value (Extended)	Parameter	Value (Ferry)	Value (Extended)
$\tau_{dist}^{\text{Peak}}$	1.000	0.800 (20%↓)	$\tau_{\Delta COG}^{\text{Peak}}$	10°/180°	5°/180° (50%↓)
τ_{dist}^{Amp}	0.600	0.500 (17%↓)	$\tau_{\Delta COG}^{\text{Amp}}$	0.200	0.100 (50%↓)
$\tau_{dist}^{\text{Prop}}$	0.400	0.200 (50%↓)	$\tau_{\Delta COG}^{\text{Prop}}$	0.300	0.200 (33%↓)
τ_{ROT}	15°/min	15°/min	$\tau_{Decline}$	0.100	-

The results show that the proposed CPD-based behaviour identification method is not restricted to the regular ferry corridor and can be applied to more diverse structured waterways. Nevertheless, the reduced performance matrix indicates that the performance of the method may decline as the heterogeneity of navigational environments increases.

5.2. Implications of extracted critical encounters

Based on the extracted critical encounters, an analysis of avoidance timing, minimum ship-to-ship distance, and maximum course alteration for give-way and stand-on ships across different crossing encounter types provides further insights relevant to the development of autonomous ship collision avoidance models. First, among the 4840 extracted critical encounter scenarios, less than 1% of cases are $Cross_{stern2bow}$ encounters, indicating that when ships are able to pass astern of the target ship while following the planned route, bow-passing avoidance behaviours are rarely adopted if circumstances permit. Second, give-way and stand-on ships exhibit similar magnitudes of maximum course alteration relative to the planned route, suggesting that ships with different responsibilities share a comparable understanding of what is "substantial action" as required by the COLREGs. Third, for stern-passing CABs, although give-way ships take evasive actions significantly earlier than stand-on ships, both responsibilities maintain highly similar minimum ship-to-ship distances. On the one hand, this suggests that the interpretation of an acceptable safety distance does not vary substantially with collision avoidance responsibility, which is consistent with navigational practice where statistic-based ship domains are not explicitly differentiated between give-way and stand-on ships. On the other hand, it indicates that although stand-on ships tend to take avoidance actions later, this delay does not lead to smaller minimum passing distances. This suggests that the avoidance timing of stand-on ships remains within a safe range, offering insight into the lower bound of acceptable avoidance timing of stand-on ships. Fourth, for bow-passing CABs, the similar avoidance timing but smaller minimum distances observed for give-way ships suggest that $Cross_{bow}$ encounters are likely associated with navigational constraints or limited manoeuvring space, which prevent early avoidance actions and hinder passing at a larger safety distance. Consequently, both the COLREGs and navigational practice indicate that, when circumstances permit, autonomous ship collision avoidance models should avoid passing ahead of other ships.

The findings provide valuable insights and implications for a range of stakeholders.

(1) Implications for the development of MASS.

The extracted critical encounter scenarios provide valuable real-world data for the development and testing of autonomous collision avoidance systems. Most existing methods, such as velocity obstacles (Wang et al., 2023), model predictive control (Chen et al., 2025), artificial potential fields (Li et al., 2024a), and reinforcement learning (Wang et al., 2024a; Yang et al., 2026), rely on expert knowledge to generate collision avoidance strategies. However, collision avoidance strategies are influenced by many factors, including the encounter scenarios, environmental conditions, and interpretation of COLREGs. Expert knowledge alone is therefore unlikely to fully reflect navigators' practical experience. The critical encounter scenarios extracted by the proposed framework, containing navigators' CABs across a wide range of real encounter conditions, can provide the data for MASSs to learn collision avoidance strategies that are more consistent with actual practical experience. Furthermore, most existing autonomous collision avoidance methods are validated using manually constructed testing scenarios, which may not reflect the complexity and diversity of typical real-world encounters. The large set of critical encounter scenarios extracted by this framework can serve as realistic test cases, enabling more rigorous and representative validation of autonomous collision avoidance systems across varied and challenging real-world conditions.

(2) Implications for enhancing maritime situational awareness.

The extracted critical encounter scenarios can also support the development of interaction-aware ship trajectory prediction models, which can significantly enhance the crew's maritime situational awareness. In historical AIS data, normal route-following trajectories account for the majority of samples, while collision avoidance interactions are relatively rare and often embedded within long periods of routine navigation. As a result, prediction models trained on general AIS data have limited ability to capture how ships interact in safety-critical encounters, making it challenging to reveal the potential future interactions of surrounding ships. By extracting critical encounter scenarios in which collision avoidance behaviour is observable, the proposed framework provides interaction-rich samples for analysing ship-to-ship interactions. These scenarios can be used to construct targeted training or evaluation datasets, helping future prediction models better assess whether they can reproduce realistic manoeuvring responses under collision avoidance situations, thereby enhancing maritime situational awareness.

(3) Implications for traffic management.

The proposed framework enables maritime authorities to systematically analyse critical encounters from historical AIS data, providing evidence that is difficult to obtain through conventional monitoring. Since most traffic conflicts are resolved through effective CABs, only a small proportion escalate into accidents due to factors such as insufficient situational awareness or faulty decision-making. Accident statistics therefore capture only a fraction of the traffic conflicts that actually occur, and do not accurately reflect the true frequency of close-quarters/near-miss/high-conflict situations in a given waterway. By detecting CABs and identifying the corresponding hotspots, the proposed framework provides a more complete picture of traffic conflict, offering an empirical basis for maritime surveillance operators to take effective measures to alleviate traffic conflicts, such as the establishment or adjustment of TSSs, the introduction of speed restrictions in congested traffic lanes, or optimisation of traffic flow management.

6. Conclusions

This paper developed a route-aware framework for detecting ship collision avoidance behaviour from historical AIS trajectories and for extracting critical encounter scenarios through avoidance intent inference. The study demonstrated that the proposed method can distinguish avoidance manoeuvres from normal route-following behaviour more reliably by incorporating planned route information and CPD. By comparing observed trajectories with virtual route-following references, the framework was further shown to support the interpretation of manoeuvre intent and the extraction of behaviourally meaningful critical encounter scenarios.

A case study conducted using AIS data from the Øresund Strait demonstrates the effectiveness and interpretability of the proposed framework. The results demonstrated the effectiveness of the proposed framework in both behaviour detection and scenario extraction. Using 1500 labelled real-world trajectories from the Øresund area, the behaviour identification method achieved an F1-score of 0.8203 and the critical encounter extraction method achieved an F1-score of 0.7443, indicating strong capability in critical encounter extraction from historical AIS data. The feature importance analysis in ship behaviour identification shows that the peak course deviation relative to the planned route plays a critical role in distinguishing CCABs from RBs, highlighting the necessity of incorporating planned route information for accurate behaviour identification, which has received limited attention in many existing approaches.

Based on the identified and intention-verified avoidance behaviours, the framework further extracted 4840 critical encounter scenarios from the study area, providing a substantial empirical basis for analysing collision avoidance decision-making and supporting representative scenario construction for MASS research. Insightful results are obtained, which directly reflect the explicit requirements of the COLREGs. The extracted encounters show that give-way ships generally take collision avoidance actions earlier than stand-on ships and exhibit a clear preference for stern-passing strategies in crossing encounters when circumstances permit, which is consistent with the rules requiring early and substantial action and advising ships to avoid crossing ahead of other ships.

Beyond these explicitly stated rules, the behavioural analysis provides insight into implicit aspects of collision avoidance practice that are not directly specified in the COLREGs. In stern-passing crossing encounters, give-way ships generally initiate evasive action at larger relative distances, with mean and median values of approximately 1.65-1.69 NM, whereas the corresponding values for stand-on ships are about 1.22-1.25 NM, indicating that give-way ships typically act around 0.4 NM earlier. Despite this difference in timing, the minimum passing distances maintained by give-way and stand-on ships remain highly similar, suggesting that navigators with different responsibilities share a broadly consistent understanding of an acceptable safety distance in practice.

Future research can be directed toward several areas. First, the current framework detects candidate collision avoidance behaviours based on change points identified by CPD. However, as CPD captures all behavioural changes regardless of their cause, manoeuvres unrelated to collision avoidance (e.g., port entry or traffic-induced speed adjustments) may be misclassified. Future work should therefore incorporate additional situational context, such as the presence and motion of surrounding ships, to improve the discrimination between avoidance and non-avoidance actions. Second, environmental factors such as wind, current, and waves are not explicitly considered. Incorporating these effects could help distinguish true avoidance manoeuvres from passive drift, thereby reducing false detections under adverse conditions. Last, one limitation of the proposed intention-informed encounter extraction algorithm is related to the attribution of avoidance intention in multi-ship encounters. In Algorithm 2, surrounding ships are examined individually by comparing the real manoeuvring trajectory with the reference route-following trajectory. The design of the algorithm is effective for identifying whether a surrounding ship is affected by the observed collision avoidance manoeuvre, but it does not fully capture the coupled nature of a multi-ship avoidance situation. In practise, a manoeuvre may be triggered by the navigator's simultaneous consideration of multiple target ships when involved in a complex situation, rather than by assessing each surrounding ship independently. As a result, the observed manoeuvre may jointly modify the passing conditions and passing distances with several nearby ships. Therefore, a small subset of ships identified by Algorithm 2 should not necessarily be interpreted as independent avoidance targets. Instead, they may reflect the coupled outcome of a multi-ship avoidance decision. Future research should develop a joint multi-ship interaction model that considers surrounding ships simultaneously, so that the relative contribution of each ship to the observed avoidance behaviour can be estimated more explicitly.

References

Ankerst, M., Breunig, M.M., Kriegel, H.-P., Sander, J., 1999. OPTICS: Ordering points to identify the clustering structure. *ACM Sigmod record* 28(2), 49-60.

Bergstra, J., Bardenet, R., Bengio, Y., Kégl, B., 2011. Algorithms for hyper-parameter optimization. *Advances in neural information processing systems* 24.

Bian, Z., Zuo, F., Gao, J., Chen, Y., Venkata, S.S.C.P., Bernardes, S.D., et al., 2021. Time lag effects of COVID-19 policies on transportation systems: A comparative study of New York City and Seattle. *Transportation Research Part A: Policy and Practice* 145, 269-283.

Chen, L., Ye, Y., Chen, P., Mou, J., 2025. Angular MPC-Based Thrust Allocation Research for All-Electric Ships Considering Wake Flow Interaction. *IEEE Transactions on Transportation Electrification*.

Chen, P., Huang, Y., Mou, J., van Gelder, P.H.A.J.M., 2018. Ship collision candidate detection method: A velocity obstacle approach. *Ocean Engineering* 170, 186-198.

Chen, X., Huang, K., Jiang, H., 2022. Detecting changes in the spatiotemporal pattern of bike sharing: A change-point topic model. *IEEE Transactions on Intelligent Transportation Systems* 23(10), 18361-18377.

Chen, Y., Liu, Z., Zhang, M., Wang, X., Fu, X., 2026. Interactive Bi-LSTM: A novel approach for multi-channel vessel traffic flow prediction. *Transportation Research Part E: Logistics and Transportation Review* 214, 105026.

Cheng, Q., Song, Q., Wang, Z., Lin, Y., Liu, Z., 2025. Capturing traffic state variation process: An analytical modeling approach. *Transportation Research Part E: Logistics and Transportation Review* 198, 104119.

Feng, Y., Yang, D., 2026. Verbal-command-driven ship trajectory prediction: a context-aware intent injection mechanism for intelligent maritime transportation. *Transportation Research Part E: Logistics and Transportation Review* 212, 104911.

Fiskin, R., Atik, O., Kisi, H., Nasibov, E., Johansen, T.A., 2021. Fuzzy domain and meta-heuristic algorithm-based collision avoidance control for ships: Experimental validation in virtual and real environment. *Ocean Engineering* 220, 108502.

Goerlandt, F., Montewka, J., Lammi, H., Kujala, P., 2012. Analysis of near collisions in the Gulf of Finland, *Proceedings of the European Safety and Reliability Conference ESREL 2011*.

Gong, J., Li, H., Jiao, H., Yang, Z., 2025. Uncertainty-aware ship trajectory prediction via Spatio-Temporal Graph Transformer. *Transportation Research Part E: Logistics and Transportation Review* 203, 104315.

Guedes Soares, C., Teixeira, A., 2001. Risk assessment in maritime transportation. *Reliability Engineering & System Safety* 74(3), 299-309.

Jia, C., Ma, J., He, M., Su, Y., Zhang, Y., Yu, Q., 2022. Motion primitives learning of ship-ship interaction patterns in encounter situations. *Ocean Engineering* 247, 110708.

Li, H., Jiao, H., Yang, Z., 2023. AIS data-driven ship trajectory prediction modelling and analysis based on machine learning and deep learning methods. *Transportation Research Part E: Logistics and Transportation Review* 175, 103152.

Li, H., Lam, J.S.L., Yang, Z., Liu, J., Liu, R.W., Liang, M., et al., 2022. Unsupervised hierarchical methodology of maritime traffic pattern extraction for knowledge discovery. *Transportation Research Part C: Emerging Technologies* 143, 103856.

Li, H., Liu, J., Yang, Z., Liu, R.W., Wu, K., Wan, Y., 2020. Adaptively constrained dynamic time warping for time series classification and clustering. *Information Sciences* 534, 97-116.

Li, H., Wang, X., Guedes Soares, C., Ni, S., 2024a. A collision-avoidance decision-making scheme based on artificial potential fields and event-triggered control. *Ocean Engineering* 306, 118101.

Li, H., Xing, W., Jiao, H., Yang, Z., Li, Y., 2024b. Deep bi-directional information-empowered ship trajectory prediction for maritime autonomous surface ships. *Transportation Research Part E: Logistics and Transportation Review* 181, 103367.

Li, H., Yang, Z., 2023. Incorporation of AIS data-based machine learning into unsupervised route planning for maritime autonomous surface ships. *Transportation research part E: Logistics and transportation review* 176, 103171.

Liang, M., Cai, Y., Chen, T., Wang, H., Meng, Q., 2025. Data-driven impact analysis of chokepoint on multi-scale maritime networks: A case study of the Taiwan Strait. *Transportation Research Part E: Logistics and Transportation Review* 200, 104179.

Liang, M., Liu, R.W., Zhan, Y., Li, H., Zhu, F., Wang, F.-Y., 2022. Fine-grained vessel traffic flow prediction with a spatio-temporal multigraph convolutional network. *IEEE Transactions on Intelligent Transportation Systems* 23(12), 23694-23707.

Liang, M., Weng, L., Gao, R., Li, Y., Du, L., 2024. Unsupervised maritime anomaly detection for intelligent situational awareness using AIS data. *Knowledge-Based Systems* 284, 111313.

Liu, Z., Chen, W., Liu, C., Yan, R., Zhang, M., 2024. A data mining-then-predict method for proactive maritime traffic management by machine learning. *Engineering Applications of Artificial Intelligence* 135, 108696.

Mou, J.M., Tak, C.v.d., Ligteringen, H., 2010. Study on collision avoidance in busy waterways by using AIS data. *Ocean Engineering* 37(5-6), 483-490.

Negenborn, R.R., Goerlandt, F., Johansen, T.A., Slaets, P., Valdez Banda, O.A., Vanelslander, T., et al., 2023. Autonomous ships are on the horizon: here's what we need to know. *Nature* 615(7950), 30-33.

Park, J., Jeong, J., Park, Y., 2021. Ship trajectory prediction based on bi-LSTM using spectral-clustered AIS data. *Journal of marine science and engineering* 9(9), 1037.

Pennetti, C.A., Fontaine, M.D., Jun, J., Lambert, J.H., 2020. Evaluating capacity of transportation operations with highway travel time reliability. *Reliability Engineering & System Safety* 204, 107126.

Qi, Y., Yang, J., Bai, A., Liu, J., 2025. A method for real-time detection of vessel abnormal behavior based on CNN-LSTM. *Expert Systems with Applications* 288, 128303.

Qu, X., Meng, Q., Suyi, L., 2011. Ship collision risk assessment for the Singapore Strait. *Accid Anal Prev* 43(6), 2030-2036.

Rong, H., Teixeira, A., Guedes Soares, C., 2019. Ship trajectory uncertainty prediction based on a Gaussian Process model. *Ocean Engineering* 182, 499-511.

Rong, H., Teixeira, A., Guedes Soares, C., 2022a. Maritime traffic probabilistic prediction based on ship motion pattern extraction. *Reliability Engineering & System Safety* 217, 108061.

Rong, H., Teixeira, A., Soares, C.G., 2020. Data mining approach to shipping route characterization and anomaly detection based on AIS data. *Ocean Engineering* 198, 106936.

Rong, H., Teixeira, A., Soares, C.G., 2024. A framework for ship abnormal behaviour detection and classification using AIS data. *Reliability Engineering & System Safety* 247, 110105.

Rong, H., Teixeira, A.P., Guedes Soares, C., 2022b. Ship collision avoidance behaviour recognition and analysis based on AIS data. *Ocean Engineering* 245, 110479.

Snoek, J., Larochelle, H., Adams, R.P., 2012. Practical bayesian optimization of machine learning algorithms. *Advances in neural information processing systems* 25.

Szlapczynski, R., Szlapczynska, J., 2017. Review of ship safety domains: Models and applications. *Ocean Engineering* 145, 277-289.

Taguchi, G., 1987. System of experimental design; engineering methods to optimize quality and minimize costs.

Truong, C., Oudre, L., Vayatis, N., 2020. Selective review of offline change point detection methods. *Signal Processing* 167.

Wang, C., Zhang, X., Gao, H., Bashir, M., Li, H., Yang, Z., 2024a. COLERGs-constrained safe reinforcement learning for realising MASS's risk-informed collision avoidance decision making. *Knowledge-Based Systems* 300, 112205.

Wang, C., Zhang, X., Gao, H., Bashir, M., Li, H., Yang, Z., 2024b. Optimizing anti-collision strategy for MASS: A safe reinforcement learning approach to improve maritime traffic safety. *Ocean & Coastal Management* 253, 107161.

Wang, L., Chen, P., Chen, L., Mou, J., 2021. Ship AIS trajectory clustering: An HDBSCAN-based approach. *Journal of Marine Science and Engineering* 9(6), 566.

Wang, S., Zhang, Y., Zhang, X., Gao, Z., 2023. A novel maritime autonomous navigation decision-making system: Modeling, integration, and real ship trial. *Expert Systems with Applications* 222, 119825.

Wang, X., Liu, Z., Yan, R., Wang, H., Zhang, M., 2022. Quantitative analysis of the impact of COVID-19 on ship visiting behaviors to ports-A framework and a case study. *Ocean coastal management* 230, 106377.

Xiao, Z., Fu, X., Zhang, L., Goh, R.S.M., 2019. Traffic pattern mining and forecasting technologies in maritime traffic service networks: A comprehensive survey. *IEEE Transactions on Intelligent Transportation Systems* 21(5), 1796-1825.

Xin, X., Liu, K., Li, H., Yang, Z., 2024. Maritime traffic partitioning: An adaptive semi-supervised spectral regularization approach for leveraging multi-graph evolutionary traffic interactions. *Transportation Research Part C: Emerging Technologies* 164.

Xin, X., Liu, K., Liu, J., Wang, W., Yang, Z., 2025a. Modeling, evaluation, and mitigation of maritime traffic complexity in complex waters. *IEEE Transactions on Intelligent Transportation Systems* 26(9), 13275-13292.

Xin, X., Liu, K., Loughney, S., Wang, J., Li, H., Ekere, N., et al., 2023. Multi-scale collision risk estimation for maritime traffic in complex port waters. *Reliability Engineering & System Safety* 240, 109554.

Xin, X., Liu, K., Yu, Y., Yang, Z., 2025b. Developing robust traffic navigation scenarios for autonomous ship testing: an integrated approach to scenario extraction, characterization, and sampling in complex waters. *Transportation Research Part C: Emerging Technologies* 178, 105246.

Yan, Z., Xiao, Y., Cheng, L., He, R., Ruan, X., Zhou, X., et al., 2020. Exploring AIS data for intelligent maritime routes extraction. *Applied Ocean Research* 101, 102271.

Yan, Z., Yang, G., He, R., Yang, H., Ci, H., Wang, R., 2023. Ship trajectory clustering based on trajectory resampling and enhanced BIRCH algorithm. *Journal of Marine Science and Engineering* 11(2), 407.

Yang, D., Wu, L., Wang, S., Jia, H., Li, K.X., 2019. How big data enriches maritime research–a critical review of Automatic Identification System (AIS) data applications. *Transport reviews* 39(6), 755-773.

Yang, L., Liu, J., Zhou, Q., Liu, Z., Wang, Y., Liu, Y., et al., 2026. Advanced autonomous collision avoidance for maritime navigation: A reinforcement learning approach with ship dynamics and environmental awareness. *Transportation Research Part E: Logistics and Transportation Review* 212, 104901.

Yip, T.L., 2008. Port traffic risks–A study of accidents in Hong Kong waters. *Transportation Research Part E: Logistics and Transportation Review* 44(5), 921-931.

Yu, Y., Liu, K., Kong, W., Xin, X., 2025. Time-evolving graph-based approach for multi-ship encounter analysis: Insights into ship behavior across different scenario complexity levels. *Transportation Research Part A: Policy and Practice* 194, 104427.

Yuan, G., Sun, P., Zhao, J., Li, D., Wang, C., 2017. A review of moving object trajectory clustering algorithms. *Artificial Intelligence Review* 47(1), 123-144.

Yuan, Y., Guo, H., Fan, Z., Peng, Y., Zhang, J., Song, X., et al., 2025. A decomposable multi-fusion spatio-temporal marine traffic flow forecasting algorithm: Taking the North Sea and Baltic Sea region as an example. *Transportation Research Part E: Logistics and Transportation Review* 203, 104340.

Zhang, J., Liu, J., Hirdaris, S., Zhang, M., Tian, W., 2023a. An interpretable knowledge-based decision support method for ship collision avoidance using AIS data. *Reliability Engineering & System Safety* 230, 108919.

Zhang, L., Chen, P., Rong, H., Mou, J., Guedes Soares, C., 2024. A novel method for extracting near-misses from AIS data involving collision avoidance behaviour. *Ocean Engineering* 301, 117466.

Zhang, M., Kujala, P., Musharraf, M., Zhang, J., Hirdaris, S., 2023b. A machine learning method for the prediction of ship motion trajectories in real operational conditions. *Ocean Engineering* 283, 114905.

Zhang, M., Montewka, J., Manderbacka, T., Kujala, P., Hirdaris, S., 2020. Analysis of the grounding avoidance behavior of a ro-pax ship in the gulf of Finland using big data, *ISOPE International Ocean and Polar Engineering Conference*. ISOPE, pp. ISOPE-I-20-4226.

Zhang, M., Montewka, J., Manderbacka, T., Kujala, P., Hirdaris, S., 2021. A Big Data Analytics Method for the Evaluation of Ship - Ship Collision Risk reflecting Hydrometeorological Conditions. *Reliability Engineering & System Safety* 213, 107674.

Zhang, W., Goerlandt, F., Montewka, J., Kujala, P., 2015. A method for detecting possible near miss ship collisions from AIS data. *Ocean Engineering* 107, 60-69.

Zhang, X., Chen, X., Yao, L., Ge, C., Dong, M., 2019. Deep neural network hyperparameter optimization with orthogonal array tuning, *International conference on neural information processing*. Springer, pp. 287-295.

Zhang, X., Zhou, S., Jiang, Z., Chu, X., Yu, C., 2025. A novel ship trajectory clustering model integrated with spatiotemporal attributes. *Ocean Engineering* 336, 121774.

Zhao, C., Li, Z., Yip, T.L., Wu, B., 2026. Enhancing ship collision risk assessment by integrating virtual ship-based shared nearest neighbor clustering and game-theoretic modeling. *Transportation Research Part E: Logistics and Transportation Review* 208, 104675.

Zhao, L., Shi, G., Yang, J., 2018. Ship trajectories pre-processing based on AIS data. *The Journal of Navigation* 71(5), 1210-1230.

Appendix A: OPTICS algorithm

The reachability plot is a key component of the OPTICS algorithm, which visualises the density-based clustering results under varying reachable distances. The OPTICS algorithm relies on two key parameters: the maximum distance to consider ε and the minimum number of points to form a cluster $MinPts$. Only if there are at least $MinPts$ points within the distance ε from a point p, the point p is defined as the core point. The core distance of point p is the distance from p to its $MinPts^{th}$ nearest neighbour, expressed as follows:

$$Distance_{Core}(p,\varepsilon,MinPts) = \begin{cases} MinPts^{th} \text{ nearest distance to Neighbors,} |N_{\varepsilon}(p)| \\ \infty\text{,otherwise} \end{cases} \quad \text{(A.1)}$$

where $|N_{\varepsilon}(p)|$ represents the number of points within the ε of point p. The reachability distance of point o relative to point p is determined as the maximum between p's core distance and the actual distance from o to p, as follows:

$$Distance_{Reachability}(o,p,\varepsilon,MinPts) = \begin{cases} \max(Distance_{Core}(p,\varepsilon,MinPts),Distance(o,p))\text{ , } p \text{ is a core point} \\ \infty\text{, otherwise} \end{cases} \tag{A.2}$$

By calculating the reachability distance of each point, the clustering results for various ε are determined. More detailed pseudocode for the OPTICS algorithm procedure is provided in (Rong et al., 2022a).

Appendix B: DTW algorithm

The core of DTW is to identify the optimal mapping between two sequences and to calculate the cumulative distance of the optimal alignment path between them. Suppose $Q = \{q_1,q_2,...,q_m\}$ and $C = \{c_1,c_2,...,c_n\}$ represent two sequences. Then, a distance matrix $A_{m\times n}$ is constructed, in which $a_{ij} = \|q_i,c_j\| \in A_{m\times n}$. Based on the matrix $A_{m\times n}$, a warping path $WP = \{wp_1,wp_2,...,wp_t,...,wp_k\}$ is defined. The WP is comprised by a set of adjacent matrix elements in $A_{m\times n}$ and the length of WP must satisfy $\max(m,n) < k \leq m + n - 1$. Additionally, the warping path must satisfy the following constraints:

- **Boundary constraint**: $wp_1 = a_{11},wp_k = a_{mn}$;
- **Continuity and monotonicity**: if $wp_{t-1} = a_{i'j'},wp_t = a_{ij}$, then $0 \leq i - i' \leq 1,0 \leq j - j' \leq 1$

According to the aforementioned constraints, the DTW can identify the path with the lowest warping distance to represent the optimal mapping and distance between two sequences, as expressed as follows:

$$DTW(Q,C) = \min\left(\sum_{t=1}^{k} \frac{wp_t}{k}\right) \tag{B.1}$$

where wp_t denotes the distance between c_i and q_j, k represents the length of the longer sequence.

Considering the constraints, the minimal DTW distance is determined by following equation:

$$\begin{cases} D(1,1) = a_{11} \\ D(i,j) = a_{ij} + \min(D(i-1,j),D(i,j-1),D(i-1,j-1)) \end{cases} \tag{B.2}$$

where $D(i,j)$ represents the cumulative distance of optimal alignment path between the two sequences.

<u>**Highlights**</u>

- Propose a novel route-aware framework for detecting ship collision avoidance manoeuvres and corresponding critical encounters.
- Integrate Change Point Detection (CPD) with route information for behaviour identification.
- Develop an intention-informed method for extracting critical encounter scenarios.

- Design a unified cost function to capture the evolution patterns of collision avoidance behaviour.

Declaration of interests

☐ The authors declare that they have no known competing financial interests or personal relationships that could have appeared to influence the work reported in this paper.

☒ The authors declare the following financial interests/personal relationships which may be considered as potential competing interests:

Zaili Yang reports financial support was provided by Horizon European Research Council. If there are other authors, they declare that they have no known competing financial interests or personal relationships that could have appeared to influence the work reported in this paper.

Author Contributions

Conceptualisation, B.Z. and H.R.; methodology, B.Z. and H.R.; software, B.Z.; validation, B.Z., H.R. and H.L.; formal analysis, H.R., H.L., and Z.Y.; investigation, B.Z. and H.R.; resources, H.R., H.L., and Z.Y.; data curation, B.Z.; writing—original draft preparation, B.Z.; writing—review and editing, H.R., H.L., and Z.Y.; visualisation, B.Z.; supervision, H.R., H.L., and Z.Y.; project administration, Z.Y.; funding acquisition, Z.Y.

All authors have read and agreed to the published version of the manuscript.